Geophysical downhole logging analysis within the shallow depth ICDP STAR drilling project (Central Italy)

Paola Montone[1] *, Simona Pierdominici[2], M. Teresa Mariucci[1], Francesco Mirabella[3], Marco Urbani[3], Assel Akimbekova[3], Lauro Chiaraluce[1], Wade Johnson[4] and Massimiliano Rinaldo Barchi[3]

[1]Istituto Nazionale di Geofisica e Vulcanologia, Roma, 00143, Italy
[2]GFZ, German Research Centre for Geosciences, Telegrafenberg, 14473, Potsdam, Germany
[3]Dipartimento di Fisica e Geologia, Università degli Studi di Perugia, Perugia, 06123, Italy (Member of CRUST - Centro inteRUniversitario per l'analisi SismoTettonica tridimensionale con applicazioni territoriali)
[4]EarthScope Consortium, Boulder, CO, 80301, USA

Correspondence to: Paola Montone (paola.montone@ingv.it)

Geophysical downhole logging analysis within the shallow depth ICDP STAR drilling project (Central Italy)

Paola Montone[1] *, Simona Pierdominici[2], M. Teresa Mariucci[1], Francesco Mirabella[3], Marco Urbani[3], Assel Akimbekova[3], Lauro Chiaraluce[1], Wade Johnson[4] and Massimiliano Rinaldo Barchi[3]

[1]Istituto Nazionale di Geofisica e Vulcanologia, Roma, 00143, Italy
[2]GFZ, German Research Centre for Geosciences, Telegrafenberg, 14473, Potsdam, Germany
[3]Dipartimento di Fisica e Geologia, Università degli Studi di Perugia, Perugia, 06123, Italy (Member of CRUST - Centro inteRUniversitario per l'analisi SismoTettonica tridimensionale con applicazioni territoriali)
[4]EarthScope Consortium, Boulder, CO, 80301, USA

Correspondence to: Paola Montone (paola.montone@ingv.it)

Abstract. The ICDP STAR drilling project aims to study the seismic and aseismic fault slip behaviour of the active low-angle Alto Tiberina normal Fault (ATF) in the Northern Apennines, Central Italy, drilling and instrumenting six shallow boreholes (maximum depth 160 m) with seismometers and strainmeters. During the STAR field work, a geophysical downhole logging campaign was carried on defining the optimal target depth for instrument deployment and formation rock characterization. In particular, the main objectives of this study were to define in situ physical properties of the rocks and the tectonic discontinuity geometry along the boreholes. The downhole logging data provide new findings and knowledge especially with regards to the physical properties such as resistivity, gamma ray and wave velocity. The collected parameters were compared to the results of literature data collected in similar lithologies, as well as with the results of logging performed in deeper wells drilled for commercial purposes. The physical properties of the Mesozoic-Early Tertiary calcareous formations show low Gamma Ray values and high compressional (Vp) and shear wave (Vs) velocities (up to 5.3 km/s and 2.9 km/s, respectively), whereas the overlying clay-rich Late Tertiary formations exhibit high Gamma Ray and low resistivity and relatively low Vp and Vs values (up to 3.5 km/s and 2.0 km/s, respectively). The results obtained from the analysis of the orientations of the tectonic structures, measured along the six boreholes, show a good agreement with the orientations of the present-day extensional stress field, NE-SW oriented. Our study allowed to bridge the gap between the physical properties obtained from literature data and those obtained from the deep wells measurements, representing a possible case history for future projects. These new outcomes represent an almost unexplored window of data and will contribute to the advancement of knowledge of the physical properties of the rocks at shallow depths, typically overlooked.

1 Introduction

The aim of the STAR drilling project (A Strainmeter Array Along the Alto Tiberina Fault System) is to study seismic and aseismic slip on active high- and low angle seismogenic normal faults (Chiaraluce et al., 2024) in Central Italy, an area affected by seismic events with magnitude up to Mw 6.6 (Fig. 1). The STAR drilling project is an international effort contributing to the infrastructural implementation of the Alto Tiberina Near Fault Observatory (TABOO-NFO) (Chiaraluce et al., 2014a, 2014b; Chiaraluce et al., 2022), a long-term research infrastructure mapped by the EPOS (European Plate Observing System) initiative as one of the European Solid Earth Science facilities providing open access data to the international community (http://www.epos-eu.org). STAR is one of the International Continental Scientific Drilling Program (ICDP)projects with a primary focus on long-term borehole monitoring of fault-zone deformation (e.g., Bohnhoff et al., 2017; Fischer et al., 2022).

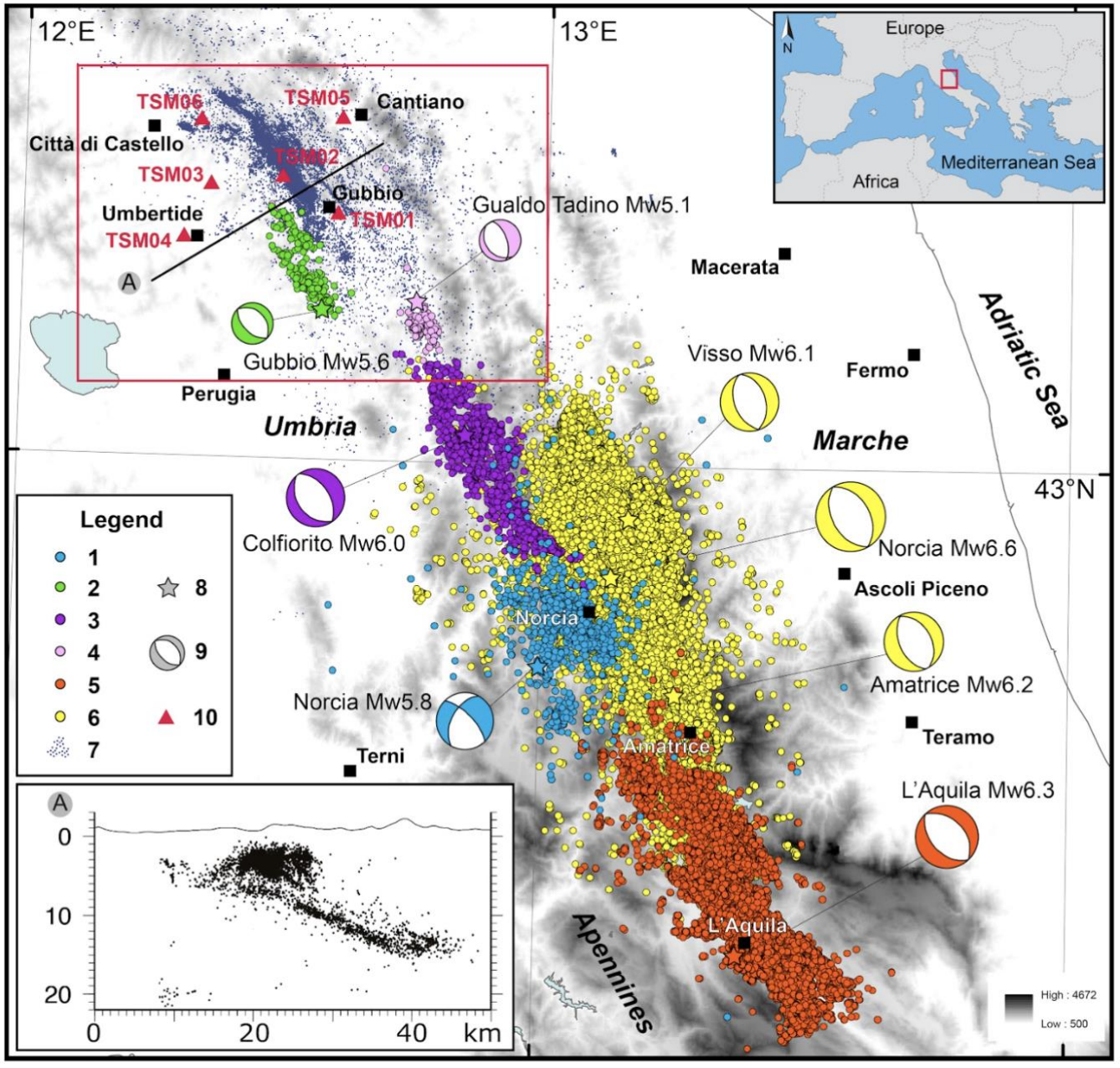

Figure 1: Seismicity in the study area and main seismic sequences in central Italy in the last 45 years. Legend: From 1 to 6: 1- Norcia 1979 (Deschamps et al., 1984); 2- Gubbio 1984 (Haessler et al., 1988); 3- Colfiorito 1997 (Chiaraluce et al., 2003); 4- Gualdo Tadino 1998 (Ciaccio et al., 2005); 5- L'Aquila 2009 (Valoroso et al., 2013); 6- Central Italy 2016-17 (Michele et al., 2020); 7- seismicity in the period 2010-2014 (Valoroso et al., 2017); 8 and 9- location of main events of the sequences and related focal mechanisms (Italian CMT dataset; Pondrelli and Salimbeni, 2006; Pondrelli et al., 2006; Quick Regional Moment Tensors); 10- STAR boreholes (TSM). The red box is the area of Figure 2. In the lower left corner, a cross section of the seismicity (Michele et al., 2020).

To improve the comprehension of the processes controlling fault mechanics and earthquake generation, the STAR drilling project installed short period (2Hz) seismometers (three-component borehole geophones) and strainmeters (Gladwin Tensor Strainmeters, GTSM) in six shallow boreholes (maximum depth 160 m) purpose-drilled. The seismometers were installed to monitor and record the seismicity of the low-angle Alto Tiberina normal Fault (ATF) and its main antithetic splay, the Gubbio normal fault (Mirabella et al., 2004; Caricchi et al., 2015) (Fig. 2). Borehole strainmeters were deployed because they are the only instruments able to measure small creep events, as demonstrated in similar experiments focused on other faults, such as the creeping section of the strike-slip San Andreas fault near Parkfield (Langbein et al., 2006). The small creep events can be recorded by strainmeters whose high resolution, for periods of hours to ~10 days, enables the identification of subtle, time-varying crustal deformations that are too small to be measured by GNSS or InSAR. Seismic and strain observations from the STAR boreholes monitoring will be integrated with regional observations on active seismicity, on deep crustal structure and on the present-day stress field.

The locations of the six boreholes were selected based on two main criteria: on a regional scale, the objective was to enhance understanding of the seismic behaviour of the ATF; on a local scale, the primary requirement was to deploy the instruments while avoiding areas of inhomogeneous, anisotropic, or highly fractured rock volumes (Chiaraluce et al., 2024). The six 80-160 m shallow monitoring boreholes, named TSM01-06, (see locations in Figure 1) were drilled surrounding the creeping portion of the ATF in two phases: during the Fall of 2021 and Spring of 2022. The STAR drilling operations were supported by the acquisition in all the boreholes of a wide set of geophysical logs including optical (OBI), acoustic (ABI), caliper (CAL), gamma ray (GR), fluid temperature conductivity (FTC), sonic (FWS), resistivity and spontaneous potential (ELOG) logs. The borehole geophysical measurement purposes for the STAR drilling project were twofold: firstly, to characterise the physical properties of the rock formation in the subsurface and, secondly, to identify an intact and competent fracture-free interval in each borehole in which to deploy the strainmeter and seismometer. After the completion, each borehole was instrumented and ready for data acquisition (Chiaraluce et al., 2024).

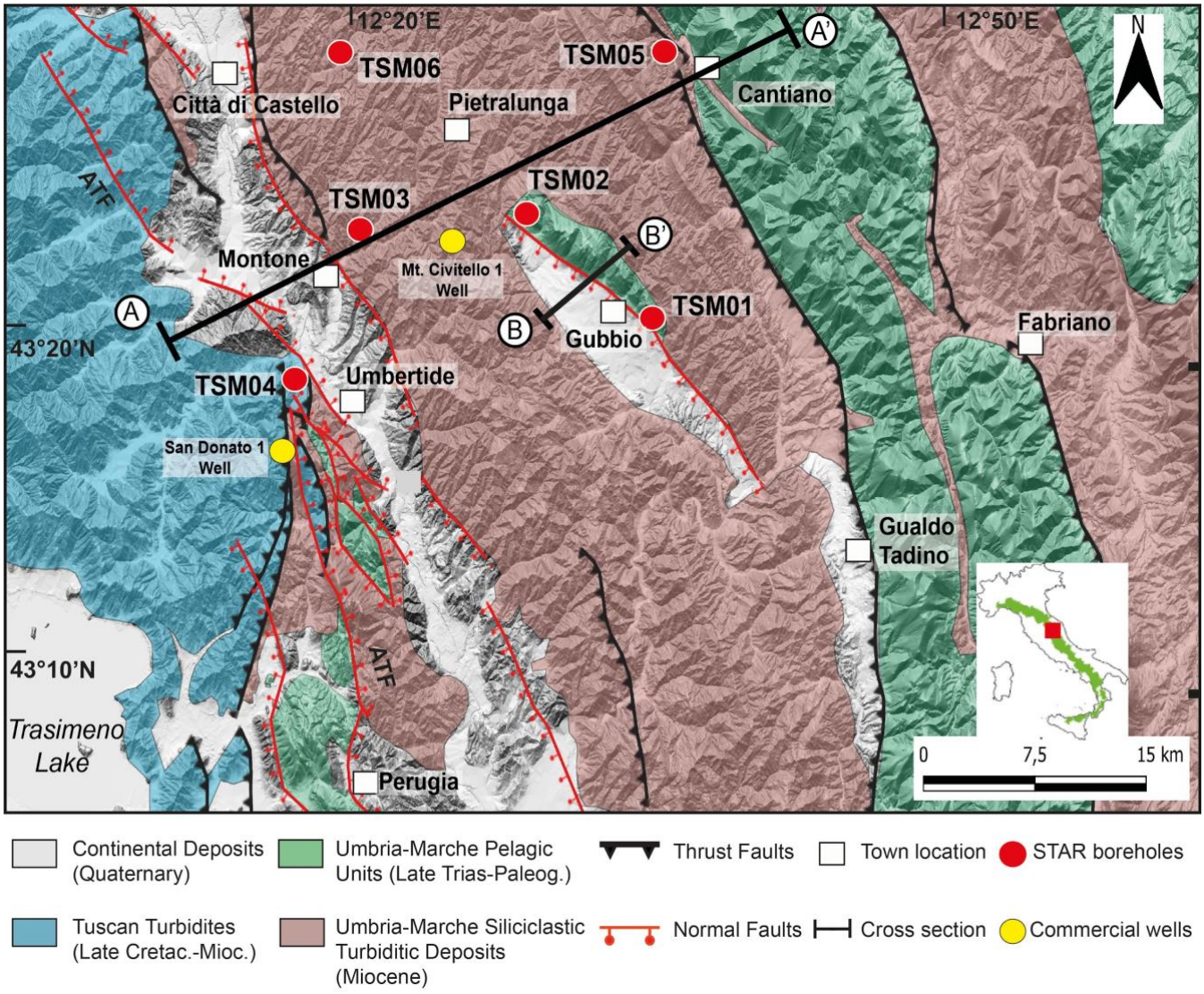

Figure 2: Geological setting of the study area. The location of the six STAR boreholes (red circles) drilled in Fall 2021 (TSM01, 02, and 03) and in Summer 2022 (TSM04, 05, and 06), and two deep commercial boreholes (yellow circles), San Donato 1 and Mt. Civitello 1, are displayed. Modified from (Mirabella et al., 2011). ATF is the Alto Tiberina fault. The geological cross-sections A-A' and B-B' are in Fig. 3.

The objective of this paper is to provide a critical overview of the physical properties of the in-situ rock formations and their fracture characteristics based on analysis and interpretation of downhole logging data. Particular attention was paid to optical and acoustic image logs with the aim of identifying intact rock and structural discontinuities. In fractured rock masses, discontinuities have significant control over the rock mass behaviour. Mapping at depth the fractures and their geometry helped us identify optimal intervals to host seismometers and strainmeters. In order to work properly and obtain reliable data, these

instruments must have a perfect coupling with the rock mass: therefore, borehole seismic installations have to take into account the borehole diameter and tilt, temperature profile, lithology and fracture distribution.

In this paper, after a brief description of the seismicity of central Italy and a geological and tectonic overview of the area where the boreholes are located, we describe the main results of the operated logging. Geophysical downhole measurements provide a contribution to better define the physical properties of the Umbria-Marche carbonate multilayer (mainly limestones and marls) and of the overlying turbidites, cropping out in this area. These results are then compared with the analogue measurements, acquired in much deeper boreholes, drilled in the same region for hydrocarbon exploration purposes, as well as with the available, recently acquired laboratory measurements (e.g. De Paola et al., 2009; Smeraglia et al., 2014; Trippetta et al., 2010, 2021), the effects of the confining pressure on the physical parameters of the rocks. In particular, the results related to the P-wave velocities obtained from the sonic log readings along the six STAR boreholes have been compared with the previous results related to the same geological formations (e.g. Barchi et al., 1998; Diaferia et al., 2006; Bigi et al., 2011; Mirabella et al., 2011; Scisciani et that give insights into al., 2014; Porreca et al., 2018; Montone and Mariucci, 2020; Trippetta et al., 2021). From the geophysical log analysis, we have defined and characterised several planar discontinuities along each borehole, related either to primary (bedding) or to secondary (tectonic) structures (fault and/or fractures). The orientations of the tectonic structures, recognized along the boreholes, have been considered together with other available data and compared with the present-day stress field.

Summarising, our paper aims to bridge the gap between the physical properties obtained from literature data (e.g. laboratory analyses) on outcrop samples and those obtained from the wellbore measurements of oil and gas companies (such as AGIP, ENI; https://www.videpi.com/videpi/pozzi/consultabili.asp), which investigate significantly greater depths. The new data of this study will contribute to the advancement of knowledge of the physical properties of the rock volumes at relatively shallow depths (0-200 m), typically overlooked. Beyond the specific case reported here, geophysical and petrophysical data acquired in shallow boreholes also contribute to the knowledge of the upper crust. Indeed, they provide in situ measurements linking those obtained on outcropping rocks, often influenced by surface processes, with those from deep wells. Our study shows how even with relatively few data in a large area, valuable insights can be obtained. With more data in a region of interest, we would be able to shed a light on a complete portion of the crust, from surface to few kilometres depth, or even deeper. Overall, also considering the results obtained in the analysis and interpretation of the data in this study, the outcomes from the STAR drilling project will provide a better understanding of the behaviour of the main active faults, addressing fundamental questions about the relationship between creep, slow slip, dynamic earthquake rupture, and tectonic faulting (Anderlini et al., 2016; Chiaraluce et al., 2024).

2 Seismotectonic and geological framework of the area

Seismicity in Central Italy is mainly characterised by shallow crustal earthquakes (5–15 km depth) localised along the Apennine belt with maximum magnitudes of about 6.6 (Chiarabba et al., 2005; Chiaraluce et al., 2017a). Earthquake focal mechanisms show a prevalent normal faulting regime, with a NE–SW striking extension, consistent with other data characterising the active stress field in this area, such as breakouts and active faults (Mariucci and Montone, 2024).

In the last 45 years, Central Italy has experienced several crustal normal-faulting earthquakes (Fig. 1) causing surface faulting as well, visible fractures and significant damage (Cinti et al., 1999; Barchi and Mirabella, 2009; Boncio et al., 2010; Emergeo working Group, 2010; Pizzi et al., 2017; Villani et al., 2018; Barchi and Collettini, 2019). The most significant earthquakes occurred in the past, with a moment magnitude greater than 5.5 (Fig. 1), are the Mw 5.8 Norcia in 1979, the Mw 5.6 Gubbio in 1984 and the seismic sequence of Colfiorito-Gualdo Tadino in 1997-98, with the largest event Mw 6.0 (Cello et al., 1997; Amato et al., 1998; Amato and Cocco, 2000; Boncio and Lavecchia, 2000; Ciaccio et al., 2005; Mildon et al., 2016). Finally, the seismic sequence that began in 2016 in Amatrice (Tinti et al., 2016; Chiaraluce et al., 2017b; Chiarabba et al., 2018) occurred with three main events (Mw 6.2 in Amatrice, Mw 6.1 in Visso, and Mw 6.6 in Norcia), causing about 300 deaths, injuries and the destruction of numerous historic centres (Fig. 1).

The six boreholes of the STAR drilling project were drilled in the NW part of the actively extending area of the Umbria-Marche Apennines (Fig. 2), a NE-verging, arc-shaped foreland fold-and-thrust belt, representing the eastern part of the Northern Apennines of Italy. Within the study area the compressional structures (folds and thrusts) are mostly arc-shaped with a roughly NNW-SSE trend and were formed in Late Miocene (Tortonian-Messinian age). They affect a pre-orogenic Jurassic-Paleogene carbonate multilayer (Umbria-Marche succession) (e.g. Cresta et al., 1989), overlain by a thick succession of syn-orogenic Neogene turbidites, marls and sandstones, deposited in the Northern Apennines foreland basin (e.g. Barchi, 2010). The compressional structures are cut and displaced by later (Late Pliocene-Quaternary) NW-SE striking normal faults, which are related to an extensional stress field oriented in a NE-direction, responsible for the present-day seismicity of the region. The normal faults attitude is consistent with the extensional stress regime inferred from earthquake focal mechanisms and borehole breakouts (Mariucci et al., 2008; Montone and Mariucci, 2016; Villani et al., 2018).

The most prominent normal fault exposed in the study area is the SW-dipping Gubbio fault, down-throwing the western backlimb of the Gubbio anticline (Fig. 3). The Gubbio fault is antithetic to a major NE-dipping extensional detachment, i.e., the ATF (e.g. Mirabella et al., 2011; Lavecchia et al., 2017; Vuan et al., 2020). The fault dip of less than 30° makes the ATF an unfavourably oriented geological structure for reactivation with respect to the regional stress field. The ATF and its high-angle antithetic splays release continuous microseismicity, and rarer moderate sequences, e.g. in 1984 (Haessler et al., 1988) and in 2010-2014 (Marzorati et al., 2014).

The stratigraphy of the study area, from top to bottom, can be summarised as follows (Barchi, 2010): i) marine and continental Plio-Quaternary sediments, mainly clays and sands in different combinations and with different degrees of compaction; ii) a thick Neogene synorogenic turbidite succession, namely Marnoso-Arenacea Fm. (Miocene), formed of alternated shales and

sandstones, with strong vertical and lateral variability; iii) a hemipelagic marly succession (Schlier, Bisciaro and Scaglia Cinerea Fms.; Eocene -Miocene); iv) a carbonate pelagic sedimentary sequence of the Umbria–Marche domain (Mesozoic–Paleogene) that includes not only limestone and chert-bearing limestone but also marl and clay (Scaglia Variegata, Scaglia Rossa, Scaglia Bianca, Marne a Fucoidi and Maiolica Fms.); v) Lower Jurassic massive platform carbonate (Calcare Massiccio Fm.); vi) Upper Triassic evaporitic succession, consisting of alternated anhydrites and dolostones (Anidriti di Burano Fm.); vii) Middle Triassic and/or older continental and shallow marine meta-sediments (Verrucano Fm. s.l.).

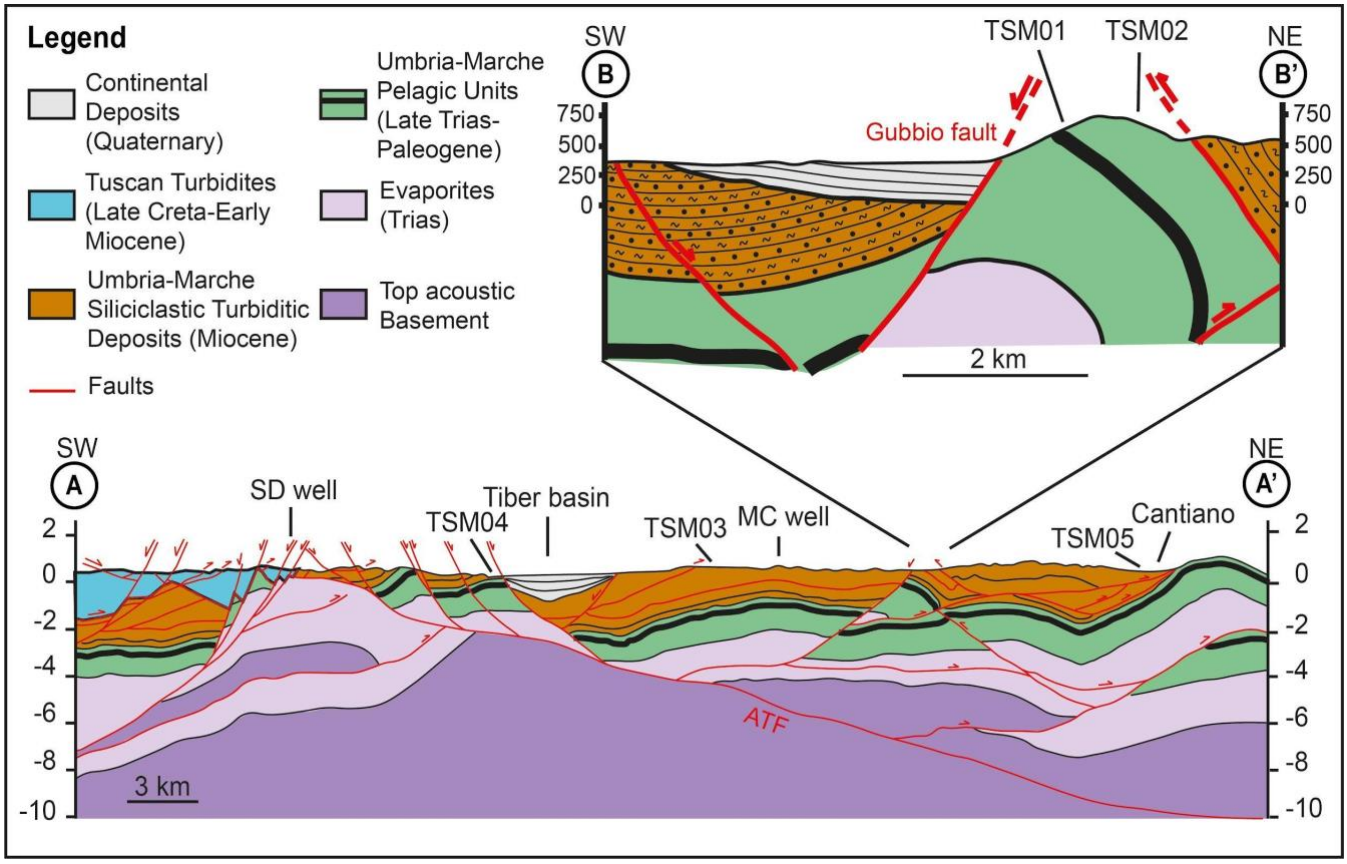

Figure 3: Geological cross-sections (A-A' and B-B' in Figure 2). The geometry at depth of the main tectonic structures such as the Alto Tiberina low angle normal fault (ATF) and the Gubbio fault (Mirabella et al., 2011) are shown. SD well, San Donato 1 well; MC well, Mt. Civitello 1 well.

Within the STAR study area (Figures 2 and 3), two deep wells (San Donato 1 and Mt. Civitello 1) were drilled in the past by Italian oil Companies. The wells stratigraphy is schematically reported in previous literature (e.g. Mariucci et al., 2008; Mirabella et al., 2011; Caricchi et al., 2015). The San Donato 1 well (SD), reaching a depth of 4763 m, was drilled by SNIA-BPD in 1983-84 and is located approximately 20 km southwest of the Mt. Civitello 1 well (MC). The SD well is situated very close to the ATF, intersecting it at a depth of 326 m, where the Miocene Marnoso-Arenacea turbidites directly overlie the

Triassic evaporitic succession, extending down to a depth of about 3000 m. At greater depth, the well penetrates the metamorphic acoustic basement in tectonic contact with the evaporitic succession (Fig. 3). The MC well, drilled by AGIP in 1988-89, located near the Gubbio fault, reaches a depth of 5600 m. From the surface to a depth of about 1000 m, the well crosses the turbidite succession. Then the well passes through the carbonate Meso-Cenozoic pelagic sequence. From about 2800 m to the bottom at 5600 m, the well crosses the Triassic evaporitic succession.

3 Method: downhole logging processing and analysis

The knowledge of the petrophysical properties of the different litho-stratigraphic units is an important aspect to understand the subsurface. In the lack of coring material, as in the STAR project, data acquisition from downhole logging becomes the key element in determining the rocks physical characterization (i.e. Rider and Kennedy, 2011). Downhole logging is a method to gain continuous, in situ high-resolution data of various physical or structural rock parameters collected within a borehole. For the STAR drilling project, the downhole logging was performed for all six boreholes in order to allow detailed sedimentary facies assessment and to identify the best location to deploy the strainmeters and seismometers at depth. All six boreholes were logged by slimhole sondes (for details see Table S1 and text in the Supplementary), and following the standard methods in this field (Serra, 1984; Ellis and Singer, 2007; Rider and Kennedy, 2011; Schön, 2015; Pierdominici and Kück, 2021). Downhole measurements were conducted in each borehole after the drilling operations and executed mainly in the open hole (OH) sections, only GR ran also in the cased section (CH). The following downhole measurements were successfully recorded: total gamma ray (GR), full waveform sonic (Vp and Vs), temperature (T) and conductivity (COND), three-arm caliper (CAL), resistivity (RESIST), single point resistance (SPR), and acoustic (ABI) and optical images (OBI). We have summarised the logging measurements and logged interval for each borehole in Table S1. For the drilling operations, water was used as drilling fluid allowing to run the OBI. Borehole quality has been determined by vertical and horizontal deviation of the borehole and the condition of the borehole wall. In order to pursue the objective of the STAR drilling project and for proper use and performance of the instruments, all six boreholes were drilled within 5° from the vertical. The deviation of each borehole was then checked as part of the logging program. The boreholes have an inclination of less than 2° except for the borehole TSM06 where the inclination is between 4.3° and 5.1°. Based on i) the smooth borehole wall, ii) log without intervals of large washouts and iii) internal consistency for several tools (i.e., three different types of borehole diameter measurement), we infer that the log quality and reliability are very good for almost all sondes over the entire length of each hole.

Below, we have summarised the main scientific purpose of each sonde.

The total gamma ray log (GR) measures the natural radioactivity of the rock. The GR comes from the radioactive isotopes of potassium (40K), uranium (238U decay series) and thorium (232Th decay series). Potassium is found primarily in clay minerals, micas, and potassium feldspar; thorium is commonly associated with clay minerals and volcanic ash layers; uranium

is found in heavy minerals, glauconite and organic rich intervals and may be bound to clay. Relatively high values in GR log are often associated with the influx of clay and coarser materials, while relatively low GR values generally indicate sedimentation of biogenic carbonate, organic carbon, or silica (e.g. Rider and Kennedy, 2011). We performed the GR log to detect layers of clay and to identify changes in lithology. GR was also recorded in drill pipes of all six STAR boreholes, although the signal appears a bit dampened. In essence, GR log characterises the different lithology crossed by the borehole allowing to identify layers (thickness and lithotype) through the different clay content.

A three-arm caliper (CAL) sonde was used to measure the borehole diameter and to determine how smooth the borehole walls are. The strainmeter requires relatively smooth walls with no blowouts or fractures.

The fluid temperature-conductivity (FTS) measures the temporary temperature and conductivity of the borehole fluid. Both parameters can show strong variations caused by drilling activities inside the hole but also can detect flow of fluids into or out of the formation. These logs are good indicators of areas of active flow or open fractures, therefore are used to exclude areas or intervals with major fractures that would have affected both instrument placement and data quality.

The ELOG sonde - including RES and SPR - measures the rock capability to conduct electric currents. The tool provides resistivity profiles with four different depths of investigation. This measurement provides information about permeability, porosity, water types and geological formation properties. In particular, in massive rocks with very low matrix porosity/permeability, the resistivity logs identify fluid filled fracture zones (fracture permeability). So, we ran this logging sonde for the same reason as the FTS. Only for the TSM01 and TSM02 boreholes the ELOG logs were not acquired.

The Full Waveform Sonic (FWS) sonde measures the velocity of sound waves through the rocks, which varies depending on lithology, rock texture and porosity. The sonic velocity measurement is used for identification of compaction of lithologies, facies recognition and fracture identification. The velocity has been determined by measuring the travel time of sonic pulses between transmitters and four receivers. We have reprocessed the raw sonic waveforms to estimate the P and S-wave velocities using a combination of first arrival trace picking for P and S waves, along with additional semblance analysis.

Borehole image sondes provide a continuous oriented high resolution image of the borehole walls (see the figures related to the boreholes, e.g., Fig. 6). Images collected in the STAR project have been obtained from acoustic (ABI) and optical (OBI) tools. The latter acquires a true-colour optical image of the borehole wall, and the acquired data are displayed in one oriented unwrapped image. The sonde operates only in a transparent drilling fluid like fresh water or air. For TSM04 and TSM06 boreholes no optical image is available due to the high turbidity of the drilling water. The acoustic image data are visualised as two 360 degrees north-oriented images (travel time and amplitude) of the borehole wall versus depth. The travel time (TT) provides information about the borehole shape and the acoustic amplitude (AMPL) depends on the roughness and shape of the borehole wall and its acoustic properties, which depend on variations with texture, mineralogy, compaction, and fracturing (e.g. Davatzes and Hickman, 2010; Mcginnis et al., 2017; Medici et al., 2023). These AMPL and TT images are visualised in colours based on their value range. Here, in the AMPL image, strong contrast (high amplitude, bright colour) indicates a strong signal and good reflection, and low contrast (low amplitude, dark colour) indicates weak to missing signals (scattered or

absorbed impulse). In the TT image, the bright colours indicate a short time period (fast) for the impulse to go from the transducer and back to the receiver; the dark colours represent a long time period (slow), which means widened size of the borehole (e.g. Pierdominici et al., 2020). Each planar discontinuity, such as fracture, fault, bedding, appears in the images as sine waves (e.g. Davatzes and Hickman, 2010). To obtain a correct geometry of the planar structures (dip azimuth and dip) the TT and AMPL images have been prior corrected by diameter, inclination and orientation of the borehole. We have grouped the features in six categories (see Section 4.3): open (in red), filled (in grey), bedding (in green), stylolite (in turquoise), cherty layer (in dark grey) and weak zones. The acoustic imager tool alone cannot distinguish between open or closed/filled structures (used here in a general term, i.e., including faults, fractures, and veins). Based on the comparison of these two images, we might distinguish so-called "open" structures based on their contrast of ultrasonic AMPL and the corresponding response in the TT. The structures defined as "closed" are visible only in the amplitude image. To enhance the travel time and amplitude images, static and dynamic (10 cm vertical window) normalizations were applied. Raw, static, dynamic images display minor differences of each other in the resulting images depending on the scale and variations between different intervals and features. The displayed images here refer to the static normalisation. The ABI and OBI were also used to determine the borehole trajectory based on borehole's deviation from vertical (DEVI) and the direction of this deviation with respect to magnetic north (hole- or drift-azimuth; HAZI). For the installation of strainmeters and seismometers, all STAR boreholes had to be very close to the vertical. Thus, this type of acquisition played a key role in knowing the condition of the borehole and decreeing the successful installation of the instruments.

4 Data and Results

4.1 Borehole description

Six STAR boreholes were drilled surrounding the creeping portion of the ATF to deploy strainmeters and seismometers (Fig. 1) in order to improve our understanding of the ATF seismicity pattern and monitor the evolution of seismicity in this area over time (Chiaraluce et al., 2024). For the location of our six boreholes, we have followed two criteria: at a regional scale, three boreholes (TSM01, 02 and 06) are located following the axis of the Gubbio anticline and its northern continuation and the others (TSM03, 04 and 05) where the maximum extension rate is expected. At a local scale, the instruments were deployed in relatively homogeneous lithology, avoiding complex formations (e.g. alternating stiff and weak rocks or limestones and marl layers) as well as anisotropic or highly fractured rock intervals. The downhole logging measurements were performed immediately after drilling and prior to instrument installation. A posteriori, the known mechanical properties of the rocks hosting the instruments will be used to improve the interpretation of the data recorded.

The boreholes are located within an area of about 1500 km^2, centred around the town of Gubbio (Fig. 2 and Table S2). TSM01 and TSM02, near the Gubbio fault, were drilled across the late Mesozoic-Early Tertiary carbonates, cropping out along the crest of the Gubbio anticline (Fig. 4 a, b). The other boreholes were drilled in the Tertiary marls and sandstones, cropping out

in the northern part of the study area: TSM04 is located on the footwall of the ATF, TSM03 and TSM06 were drilled on the ATF hangiwall, and TSM05 is located in the farthest part of the ATF, close to the western flank of the Umbria-Marche ridge (Fig. 4 c, d, e and f; for more detail, see Chiaraluce et al., 2024). See supplementary files for a lithological detailed description (Supplementary 1).

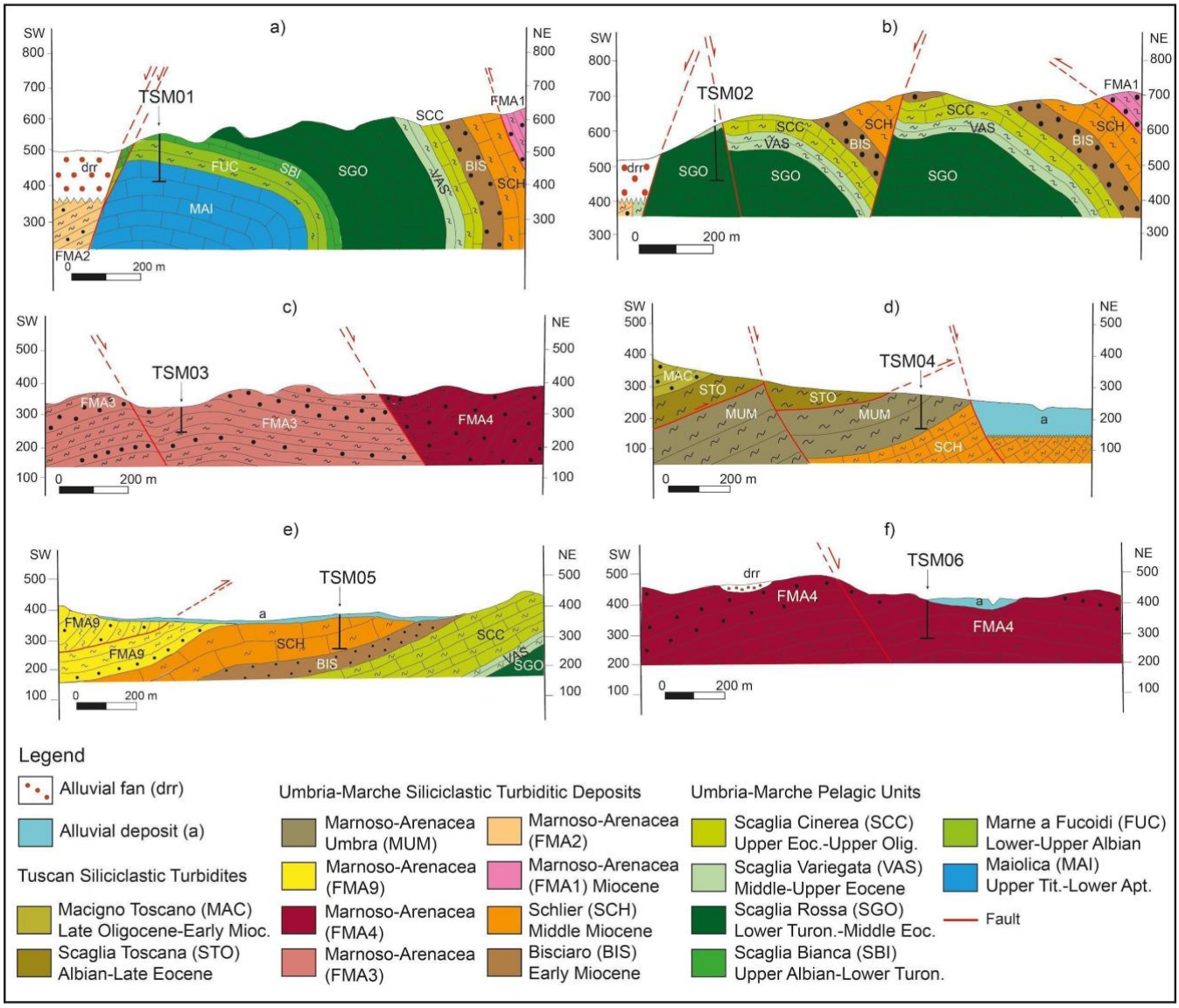

Figure 4: Geological cross-sections across the STAR boreholes. Different members of Marnoso-Arenacea Fm. are shown (FMA1, 2, 3, 4, 9 and MUM).

4.2 Log results

The downhole logging data are described and interpreted to provide new findings and knowledge to complement those obtained from similar rock types sampled in the field outcrops (Fig. 5 and Figs. 6-9).

Results from the downhole logging analysis are summarised in Table 1 and Table S1 displaying the average values and the related standard deviation. More details are described in Supplementary 2.

Boreholes	ICDP-ID	Lithological Formation*	Depth m		GR cps		Vp m/s	Vs m/s	RES Ωm	SPR Ωm	T °C	COND µS/cm
			CH	OH	CH	OH						
TSM01	5070_1_A	Maiolica	0.0-99.3	99.3-133.0	17.9±13.3	8.4±4.4	5324±371	2885±112	n.d	n.d	12±1	381±40
TSM02	5070_2_A	Scaglia Rossa	0.0-97.0	97.0-160.3	11.7±5.4	13.4±5.6	4867±184	2505±500	n.d	n.d	15±1	456±62
TSM03	5070_3_B	Marnoso-Arenacea	0.0-32.0	32.0-80.0	61.5±12.7	104.2±15.9	3204±168	1800±130	29±5	104±10	14±0.2	452±7
TSM04	5070_4_A	Marnoso-Arenacea	0.0-79.3	79.3-101.0	61.5±10.0	85.1±13.2	2972±207	1993±118	9±1	42±5	16±0.3	694±92
TSM05	5070_5_A	Schlier	0.0-82.3	82.3-118.0	48.6±8.7	81.2±9.3	3451±160	1879±148	12±3	53±7	17±1	634±8
TSM06	5070_6_A	Marnoso-Arenacea	0.0-80.0	80.0-117.5	62.4±9.2	99.7±9.35	3422±306	1896±119	18±3	76±9	18±0.03	487±34

Table 1: Geophysical properties of the rocks for TSM boreholes. GR: gamma ray (count per second); Vp and Vs: P- and S wave velocity, respectively; RES: resistivity; SPR: single point resistance; T: temperature; COND: conductivity; CH: cased hole; OH: open hole. *The lithological formations refer to the open hole section. n.d stands for no data

GR log response (open and cased hole) in TSM01 and TSM02 boreholes is generally very low (Fig. 5, Table 1). In TSM01, the low GR, associated with the limestone Scaglia Bianca Fm., slowly increases in the marly Marne a Fucoidi Fm., proportionally to the enrichment of the clay component as well evidenced in the interval between 55.0 m and 66.5 m. The sharp contact between the Marne a Fucoidi Fm. and the underlying limestone Maiolica Fm. is well indicated by the dramatic decrease in GR values (from 50 cps of Marne a Fucoidi Fm. to 14 cps of Maiolica Fm.). The open-hole section interests only the Maiolica Fm. with an average GR value of 8.4 cps. In TSM02, GR records a very low response related to the three pelagic formations intersected, predominantly consisting of limestones, which are interbedded with sporadic, relatively thin marly layers as recorded by the increase in GR values (e.g. 73-75 m, 102-104 m, 134-135 m in Scaglia Rossa Fm.). In the TSM03, TSM04, TSM05 and TSM06 boreholes, GR log shows higher values which vary between 49 cps in TSM05, and 104 cps (open hole) in TSM03. The GR values are lower in the cased section because the signal is damped by casing. In the open-hole section, on the other hand, the GR response for all the four boreholes is generally high, displaying relatively uniform cps value ranging between 81 and 104. Intervals with low GR are few and restricted and likely associated with the presence of fractures and/or thin sandstone layers. The highest GR values are almost exclusively associated with the marly layers that dominate the Marnoso-Arenacea Fm. (TSM03, TSM04 and TSM06) and the Schlier Fm. (TSM05).

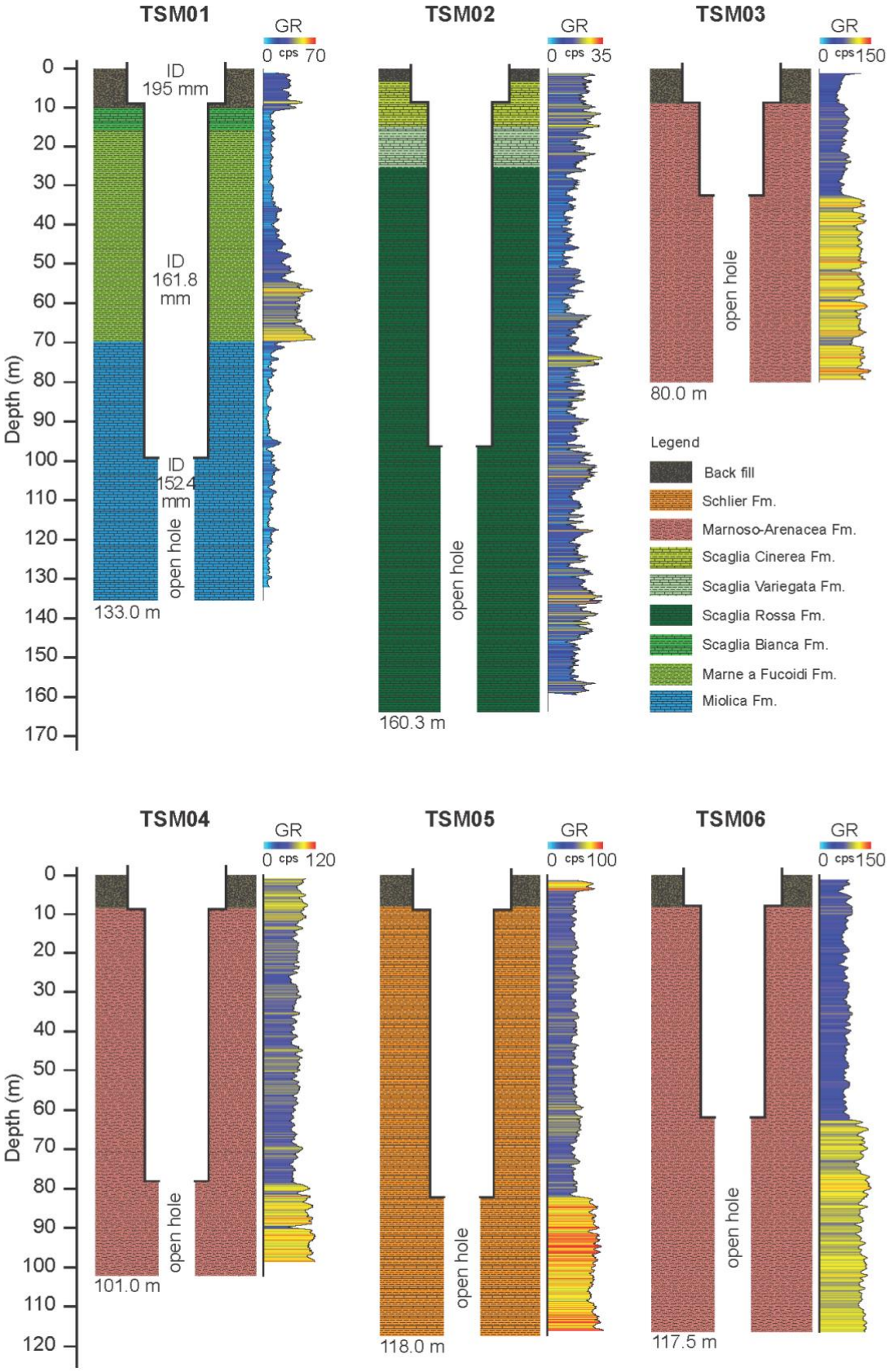
TSM01
GR
0 cps 70
ID
195 mm
ID
161.8
mm
ID
152.4
mm
open hole
133.0 m
Depth (m)
0
10
20
30
40
50
60
70
80
90
100
110
120
130
140
150
160
170
TSM02
GR
0 cps 35
open hole
160.3 m
TSM03
GR
0 cps150
open hole
80.0 m
Legend
Back fill
Schlier Fm.
Marnoso-Arenacea Fm.
Scaglia Cinerea Fm.
Scaglia Variegata Fm.
Scaglia Rossa Fm.
Scaglia Bianca Fm.
Marne a Fucoidi Fm.
Miolica Fm.
TSM04
GR
0 cps 120
open hole
101.0 m
Depth (m)
0
10
20
30
40
50
60
70
80
90
100
110
120
TSM05
GR
0 cps100
open hole
118.0 m
TSM06
GR
0 cps150
open hole
117.5 m

288

Figure 5: STAR boreholes with lithostratigraphic profile and gamma-ray log. Each borehole has a conductor casing for the first 9 m, followed by a casing and an open-hole section. ID: inner diameters. Only the total gamma (GR, here shown; unit: cps - counts per second) was also run through the casing, while all other measurements were performed only in the open hole. Seismometers and strainmeters were deployed at the bottom of the open section of each borehole (for details see Fig. S1).

P (Vp) and S (Vs) wave velocities obtained from the full wave sonic log were measured in the open–hole section down to the bottom of the hole showing a wide range of values between different boreholes: Vp varies between 2972 and 5324 m/s and Vs between 1800 and 2884 m/s (Table 1; Figs. 6-9). Higher values were recorded along the boreholes that intersected more competent lithologies, especially limestones as Maiolica Fm. in TSM01 and Scaglia Rossa in TSM02. A significant decrease of both Vp and Vs was detected at open fractures occurrence. The dynamic Poisson ratio was computed using the specific formula from shear and compressional wave velocities from sonic logs to compare it to the fracture porosity. As expected, rocks with a low Poisson's ratio show a higher fracture density (Figs. 6-9).

Resistivity was measured in TSM03, TSM04, TSM05 and TSM06 boreholes. The values vary from 9 to 29 Ωm according to the response of sonic logs and fracture presence (Table 1); however, with the same lithology the resistivity values vary following the variations of single point resistance (SPR).

Temperature measured in the boreholes (Table 1) is quite constant within a range of 12 to 18°C reflecting the borehole fluid rather than the “formation temperature”. Due to the shallow investigated depth, the results are not very significant. See Section 3 for details.

Conductivity of the drilling fluid is directly proportional to the concentration of dissolved minerals and thus to its salinity: the highest values (694 μS/cm) were found in the TSM04 borehole near the area with intense CO2 emissions of deep origin (Table 1).

4.3 Structure analysis

In this section we present the analysis of optical and acoustic images performed to identify the main discontinuities along the boreholes (Figs. 6-9). As mentioned before, we have grouped the features in six categories: open (in red), filled (in grey), bedding (in green), stylolite (in turquoise), chert layer (in dark grey) and weak zones. The filled and open fractures usually have a thickness from a few mm up to 1-2 cm. Furthermore, we plotted the main tectonic structures (open and filled fractures and weak zones) as rose diagrams splitting the data according to their dipping (> and < 45°).

TSM01. The analysis of OBI and ABI images allowed us to identify and detect the main discontinuities crossed by the borehole (Fig. 6). The sub-horizontal discontinuities correspond to bedding planes, while the filled discontinuities can be interpreted as later-filled fractures or cleavage planes. Moreover, numerous stylolites and chert layers are present within the Maiolica Fm., both parallel to bedding. A detail of the main features is shown in the inset of Fig. 6-i. A total of 69 discontinuities (only open and filled fractures) were recorded along the open-hole section showing a homogeneous distribution along the borehole with

322 a maximum of 8 structures per metre. The preferential orientation is NW-SE, corresponding to a dip azimuth of N200° (Fig.
323 10). The dip of these planes is generally low (around 25°), contributing to the azimuthal dispersion of the data. However, some
324 discontinuities with steeper dips (ranging from 60° to 80°) are still NW-SE oriented.
325

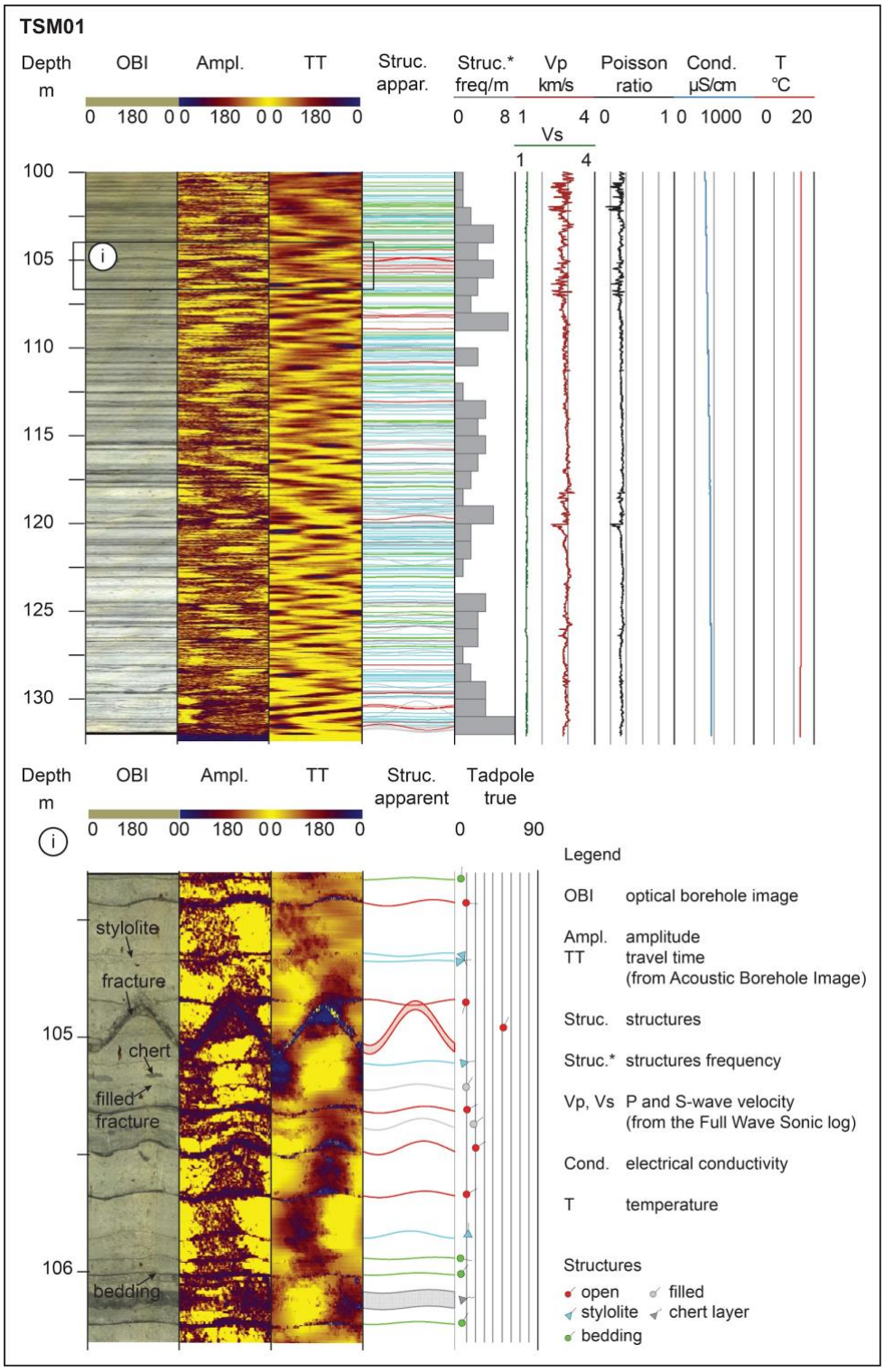
TSM01
Depth m
OBI
Ampl.
TT
Struc. appar.
Struc.* freq/m
Vp km/s
Vs
Poisson ratio
Cond. µS/cm
T °C
0 180 0 0 180 0 0 180 0
0 8 1 4 0 1 0 1000 0 20
1 4
100
105
110
115
120
125
130
i
Depth m
OBI
Ampl.
TT
Struc. apparent
Tadpole true
0 180 00 180 00 180 0
0 90
stylolite
fracture
chert
filled fracture
bedding
105
106
Legend
OBI optical borehole image
Ampl. amplitude
TT travel time
(from Acoustic Borehole Image)
Struc. structures
Struc.* structures frequency
Vp, Vs P and S-wave velocity
(from the Full Wave Sonic log)
Cond. electrical conductivity
T temperature
Structures
open
filled
stylolite
chert layer
bedding

326

Figure 6: Downhole logging measurements performed along the TSM01 borehole (Maiolica Fm.). At the bottom: a detail of the structures intersected by the borehole.

TSM02. The OBI and ABI images available for structural analysis investigated two different depth ranges. The OBI was performed from 96.2 to 147.0 m and the ABI from 144.2 to 159.6 m. The OBI image clearly shows continuous and parallel layering and especially the interlayering of thin clay layers in the limestone. The Scaglia Rossa Fm. is also affected by numerous thick filled and open fractures. The analysis of the planar discontinuities identified on both images allowed us to distinguish bedding planes, filled and open fractures (Fig. 7). The latter two structures (195 counts) revealed a predominant orientation of NNW-SSE, corresponding to a dip azimuth of N204° (Fig. 10), with an average structure frequency of 6 per metre and a high discontinuities concentration around 120 to 125 m (Fig. 7-i). The majority of open and filled fractures have dipping values higher than 45°, the open ones dipping almost exclusively to NE, and the closed ones to SW (Fig. 10).

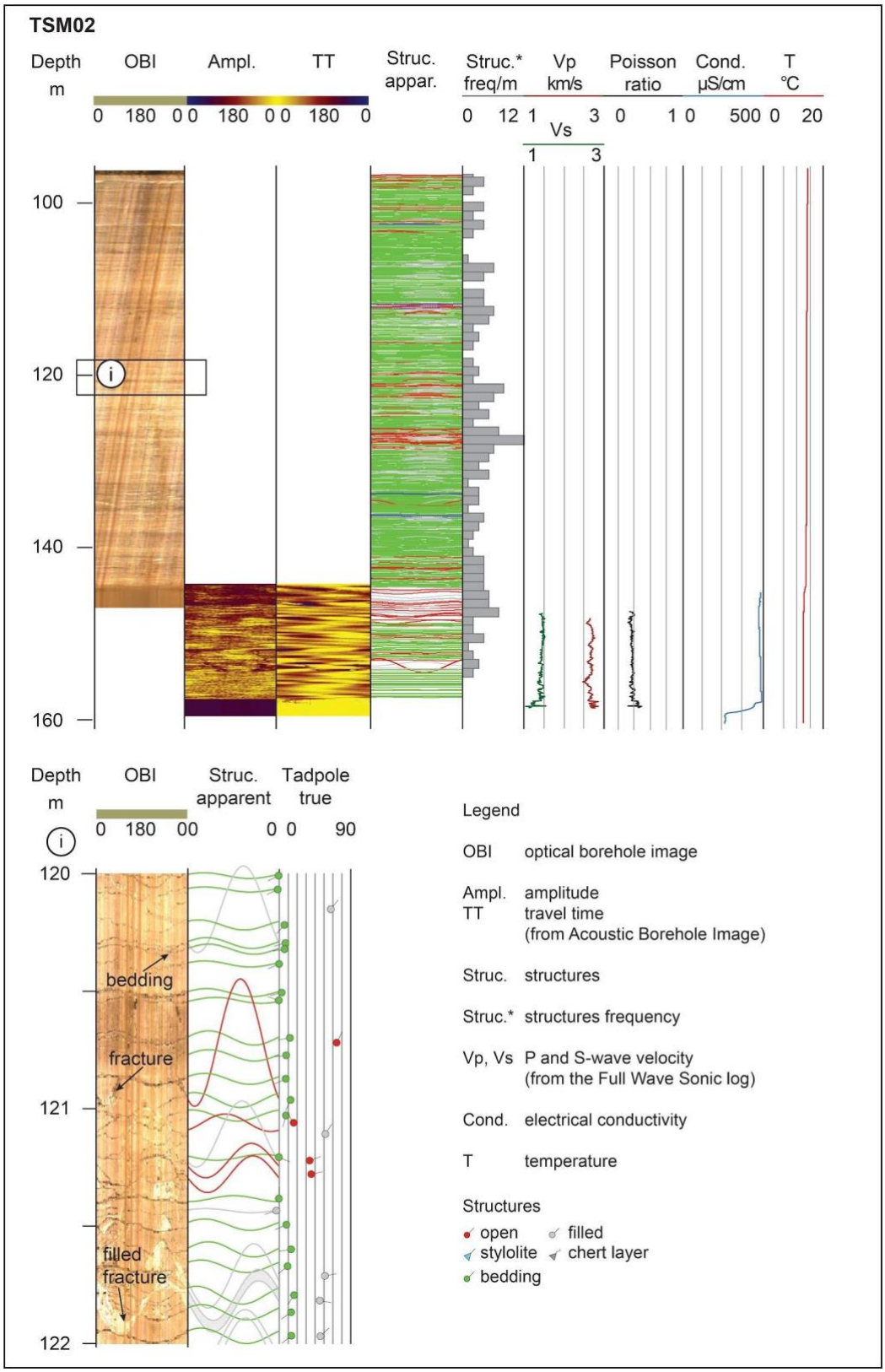
TSM02
Depth
m
OBI
Ampl.
TT
Struc.
appar.
Struc.*
freq/m
Vp
km/s
Poisson
ratio
Cond.
µS/cm
T
°C
0 180 0 0 180 0 0 180 0
0 12 1 3 0 1 0 500 0 20
Vs
1 3
100
120
140
160
i
Depth
m
OBI
Struc.
apparent
Tadpole
true
0 180 00 0 0 90
120
121
122
bedding
fracture
filled
fracture
Legend
OBI optical borehole image
Ampl. amplitude
TT travel time
(from Acoustic Borehole Image)
Struc. structures
Struc.* structures frequency
Vp, Vs P and S-wave velocity
(from the Full Wave Sonic log)
Cond. electrical conductivity
T temperature
Structures
open
filled
stylolite
chert layer
bedding

Figure 7: Downhole logging measurements performed along the TSM02 borehole (Scaglia Rossa Fm.). At the bottom: a detail of the structures intersected by the borehole.

TSM03. The poor quality of the OBI and ABI images made it difficult to perform a successful structural analysis. The unclear images are related to the high turbidity of the fluid in the borehole due to non-flushing of the borehole prior to acquisition and the high speed of running the OBI and ABI probes. Only the bedding planes were recognized showing a mean orientation of NW-SE (dip azimuth of N201°) with a very low dip of 11°. Owing to the low quality of the images, a geological survey was performed to measure bedding and main tectonic structures directly on the Marnoso-Arenacea outcrop near the drilling site (Fig. S2). Bedding varies from N204 near the borehole, to N167 and N155, dipping about 5-15°W, consistent with what was observed from the data analysis along the borehole. The thickness of the sandstone levels of Marnoso-Arenacea Fm. is up to 100-120 cm, while the thickness of the grey marly layers ranges from 1 to 10 cm; they are laminated with cleavage planes sub-parallel to the bedding. There are fractures and sometimes sub-vertical faults, which are clearly visible in the sandstone layers, with an average fracture orientation of N050 sub-vertical, N215 sub-vertical faults with extensional displacement, N213 dipping 76°W with left-lateral striae overlapped with oblique striae (pitch 55°, Fig. S2).

TSM04. The borehole intersected numerous discontinuity planes along the entire length of the measured log (Fig. 8). Although the log length is approximately only 20 m (79.8 to 100 m), the quality of the ABI images is significantly better compared to the TSM03 and TSM06 boreholes drilled in the same formation (Marnoso-Arenacea Fm.). The drastic decrease of cloudy fluid in the borehole is the combined result of wellbore flushing operations before starting log acquisition, and the low running speed of the ABI probe resulting in a good ABI image quality. 195 discontinuities between filled and open have been detected on image log with an average orientation of N184 and dipping never exceeding 60° (Fig. 10). In the field, upstream of the drilling site (Fig. S2), it was possible to measure bedding that is N180 oriented, dipping 25°W related to a small Late Cretaceous-Early Miocene outcrop of Tuscan turbidites (Fig. 2).

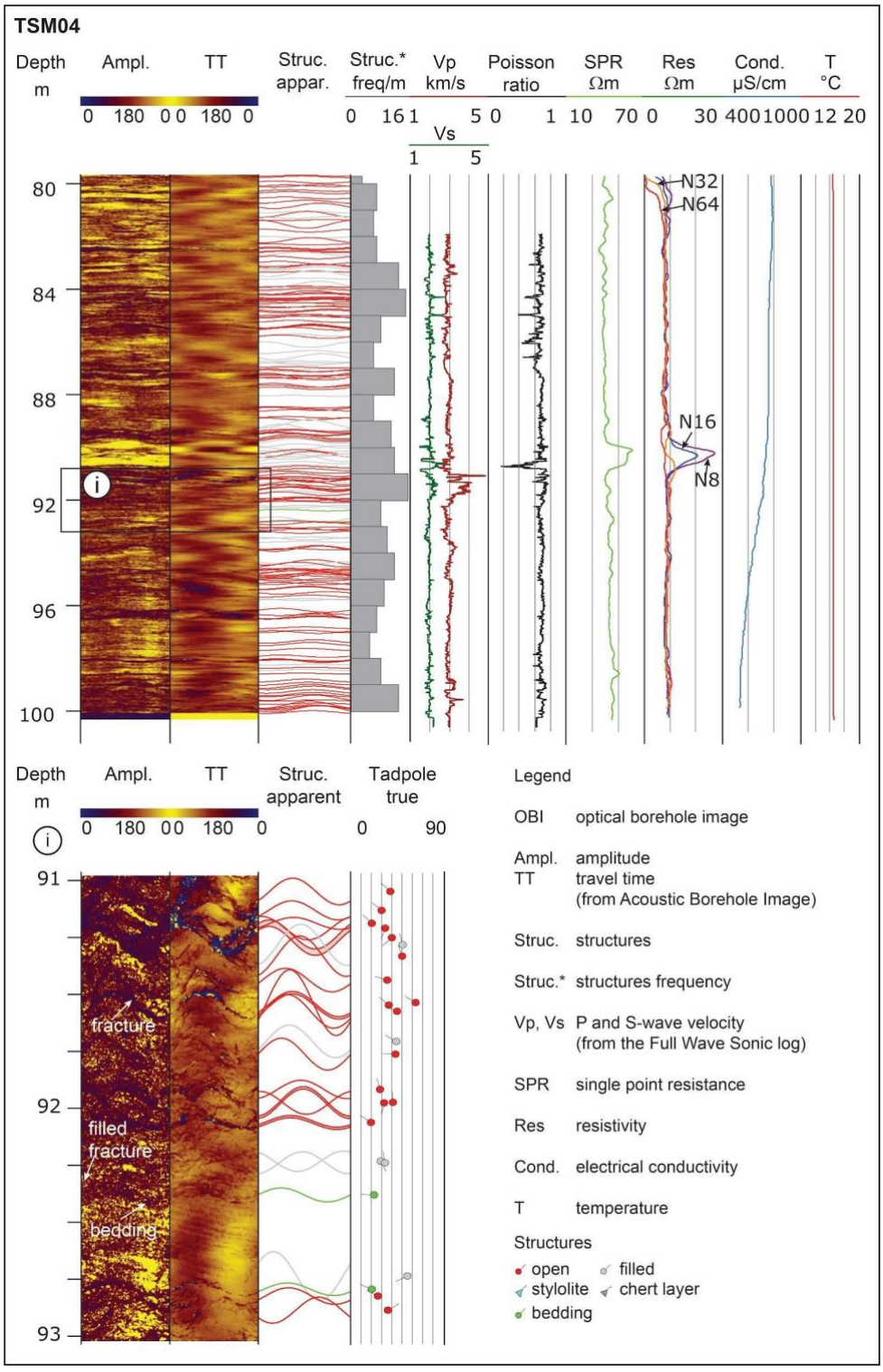
TSM04
Depth m
Ampl.
TT
0 180 0 0 180 0
Struc. appar.
Struc.* freq/m
0 16
Vp km/s
1 5
Vs
1 5
Poisson ratio
0 1
SPR Ωm
10 70
Res Ωm
0 30
Cond. µS/cm
400 1000
T °C
12 20
80
84
88
92
96
100
N32
N64
N16
N8
i
Depth m
Ampl.
TT
0 180 0 0 180 0
Struc. apparent
Tadpole true
0 90
i
91
92
93
fracture
filled fracture
bedding
Legend
OBI optical borehole image
Ampl. amplitude
TT travel time (from Acoustic Borehole Image)
Struc. structures
Struc.* structures frequency
Vp, Vs P and S-wave velocity (from the Full Wave Sonic log)
SPR single point resistance
Res resistivity
Cond. electrical conductivity
T temperature
Structures
open
filled
stylolite
chert layer
bedding

362

Figure 8: Downhole logging measurements performed along the TSM04 borehole (Marnoso-Arenacea Fm.). At the bottom: a detail of the structures intersected by the borehole. N means normal resistivity. The numbers [8, 16, 32 and 64] indicate the distance in inches between the electrode reference measuring point to the injection electrode in the resistivity sonde.

TSM05. Analysis on OBI and ABI images allowed to clearly identify tectonic structures such as open and filled structures (Fig. 9). The bedding planes instead are dubious and difficult to recognize. Discontinuity planes show a spacing quite dense (12 planes per 1 m) up to 94.8 metres; below, they are very sparse, with sections of up to 3 m without discontinuity probably also due to the acquisition and to the presence of cloudy drilling fluid in the borehole. From the image analysis a total of 114 planar structures have been identified with very consistent NW-SE orientation (corresponding to a dip azimuth of N219; Fig. 10). From this dataset, we have marked at least 4 different categories of discontinuity according to their dip, the presence or absence of filling and their aperture. A first category of discontinuities is characterised by dip greater than 45° which is related to both open and filled fractures. They show planes approximately NW-SE oriented with dip both towards SW and towards NE. The filled fractures with dip less than 45° show a similar NW-SE trend as well as the open fracture zones including wider zones (decimetre thicknesses up to 1 m; Fig. 9-i) still have a NW-SE orientation and dips ranging from very low to almost vertical. The bedding planes are mainly sub-horizontal.

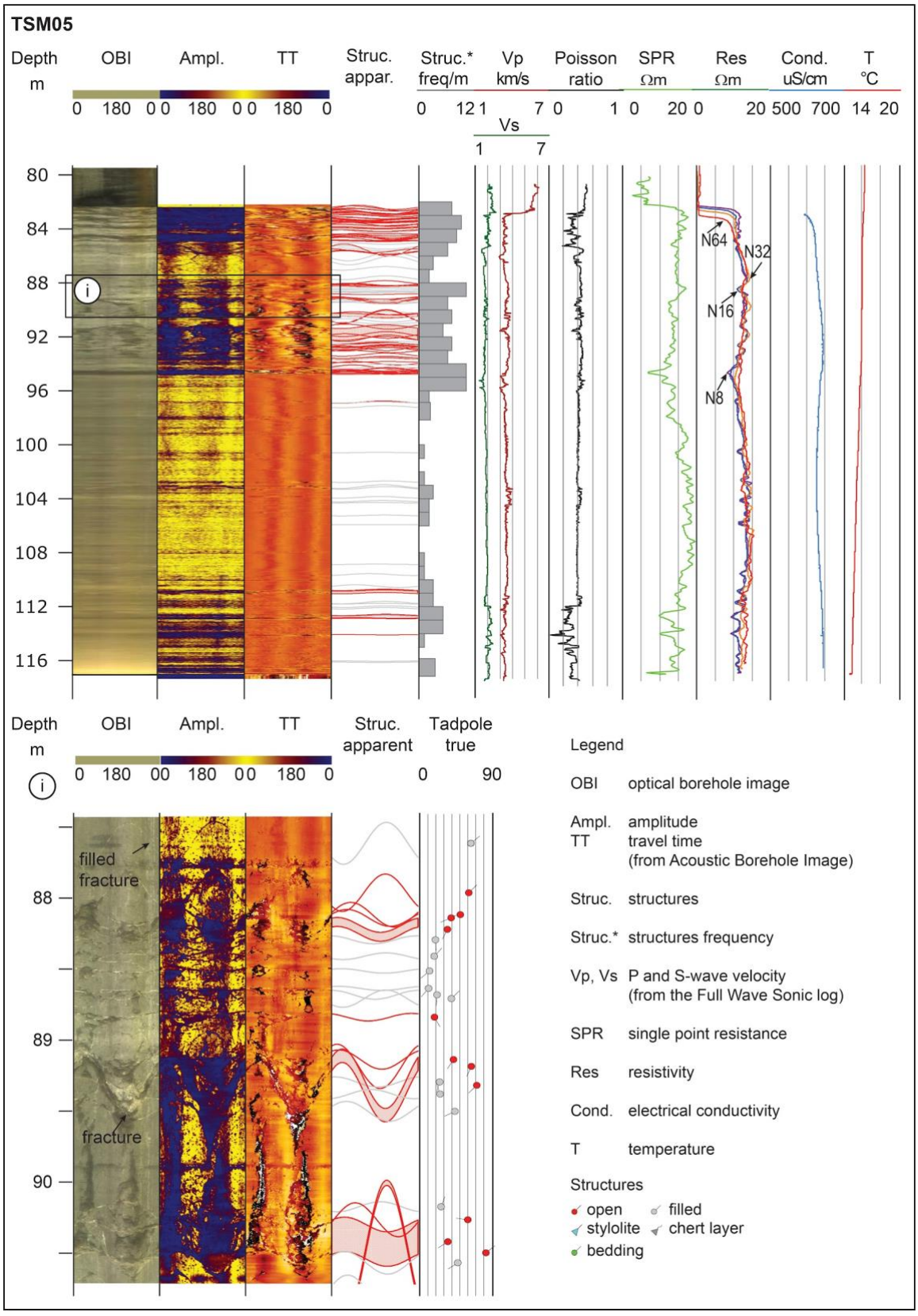
TSM05
Depth
m
OBI
Ampl.
TT
Struc.
appar.
Struc.*
freq/m
Vp
km/s
Vs
Poisson
ratio
SPR
Ωm
Res
Ωm
Cond.
uS/cm
T
°C
0 180 0 0 180 0 0 180 0
0 12 1 7 0 1 0 20 0 20 500 700 14 20
1 7
80
84
88
92
96
100
104
108
112
116
i
N64
N32
N16
N8
Depth
m
OBI
Ampl.
TT
Struc.
apparent
Tadpole
true
0 180 00 180 00 180 0
0 90
i
filled
fracture
fracture
88
89
90
Legend
OBI optical borehole image
Ampl. amplitude
TT travel time
(from Acoustic Borehole Image)
Struc. structures
Struc.* structures frequency
Vp, Vs P and S-wave velocity
(from the Full Wave Sonic log)
SPR single point resistance
Res resistivity
Cond. electrical conductivity
T temperature
Structures
open
filled
stylolite
chert layer
bedding

379

Figure 9: Downhole logging measurements performed along the TSM05 borehole (Schlier Fm.). At the bottom: a detail of the structures intersected by the borehole. N means normal resistivity. The numbers [8, 16, 32 and 64] indicate the distance in inches between the electrode reference measuring point to the injection electrode in the resistivity sonde.

TSM06. The structural analysis has been performed only on ABI image log allowing to identify 68 planar structures of which 27 open and 41 filled in the Marnoso-Arenacea Fm. (Fig. 10). The planar discontinuities show a prevailing NE-SW orientation, and dip 20-30°W. There is also a minor NNW-SSE oriented data concentration characterised by steeper dip up to 60°NE. A weak zone oriented N300 dipping 54°NE with a width of about 21 cm, has also been identified along the TSM06 borehole. In the field very close to the drilling site, bedding is N190 oriented, dipping 30°W. In the surroundings, low angle bedding planes are also NW and NE oriented. Fracture planes are N125 oriented, dipping 88°S close to the drill; other high angle tectonic structures are also E-W and NE-SW (Fig. S2).

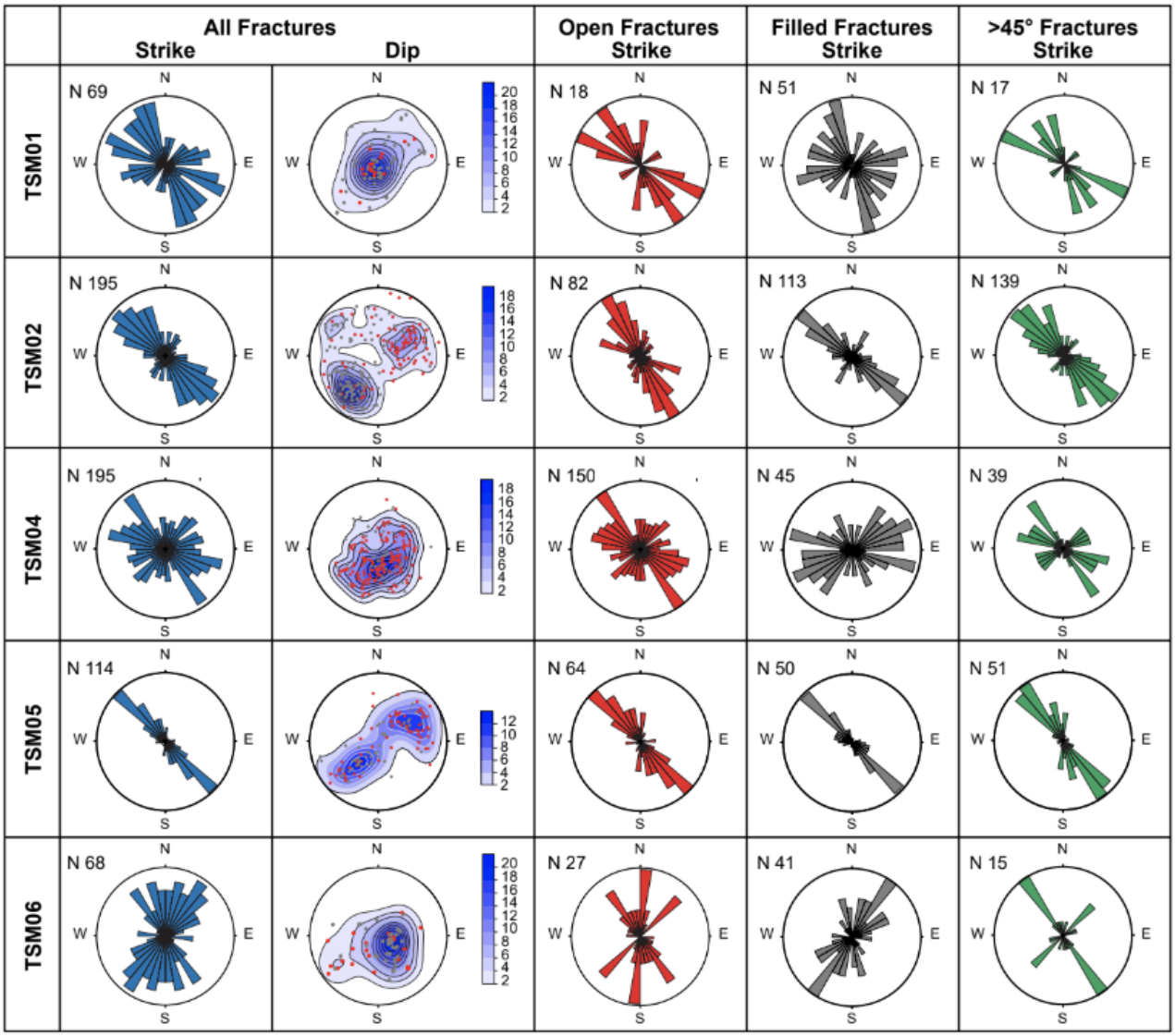

Figure 10: Rose diagrams and polar projections related to open and filled structures detected along the STAR boreholes (except TSM03). N: number of structures; DIP: poles of the planes (lower hemisphere) with the contouring (in percentage). The last column represents the fractures dipping >45°.

5 Discussion and Conclusion

In the framework of the STAR project, six shallow boreholes were drilled, conducting accurate geophysical downhole logs , aimed to identify the most suitable depth in each borehole for the deployment of seismometers and strainmeters. The results

of the seismometer and strainmeter network will require more time to obtain useful information for the project itself, dedicated to the study of the brittle upper crust, and the structure and behaviour of the Alto Tiberina low-angle seismogenic normal fault, in particular. This paper pertains solely to the initial phase of the STAR project, specifically focusing on the analysis of downhole geophysical well logs.

Downhole logging was the only way to characterise the borehole section, allowing the physical and structural properties of each geological formation to be determined, due to the lack of core samples. These in situ measurements are sensitive to formation properties on a scale that is intermediate between those obtained from literature data analysis performed on core or outcrop samples and deep geophysical measurements, performed by exploration and production drilling companies. Most geophysical and petrophysical data available in the literature come either from rock samples, analysed in the laboratories, or from well-logs, acquired along deep wells, whereas our data from geophysical logging of shallow boreholes provides an almost untapped source of information.

5.1 Physical properties

Regarding the calcareous formations of Maiolica and Scaglia Rossa Fms., crossed by the boreholes TSM01 and TSM02, respectively, the physical properties of these competent rock types are well reflected by the acquired log data (Table 1), showing low average GR values (less than 18 cps) and relatively high average values of Vp (5.3 and 4.9 km/s, respectively) and Vs (2.9 and 2.5 km/s, respectively). The almost pure limestones of the Maiolica Fm. are characterised by lower GR and higher Vp and Vs values, in comparison with the Scaglia Rossa Fm., where the clay content is significantly higher (up to 20% in the Tertiary upper portion of the Scaglia Fm., e.g. Arthur and Fischer, 1977).

The TSM03, TSM04, TSM05 and TSM06 boreholes were drilled in the marly intervals of the Neogene successions of the Marnoso-Arenacea Fm. and Schlier Fm. (TSM05). These clay-rich rocks are coherently characterised by high average GR (between 81 cps in the Schlier Fm. and 104 cps in the Marnoso-Arenacea Fm., TSM03) and low RES (between 9 Ωm and 29 Ωm). The measurements include lower values for TSM04 (9 Ωm) and TSM05 (12 Ωm), Marnoso-Arenacea and Schlier respectively, intermediate values for TSM06 (18 Ωm), and higher values (up to 29 Ωm) for TSM03.

In greater detail, the average values are not totally representative of these complex formations, typically consisting of alternated marls and sandstones: similar suggestion derives from the relatively low Vp (3.0 to 3.5 km/s) and Vs (1.8 to ~2.0 km/s) values. The temperature recorded in the boreholes (Table 1) is rather constant with values between 12°C and 18°C without showing any significant variations related to e.g. outflow or inflow zones. Unfortunately, the shallow depth of the investigation limits the significance of the results.

We compared our RES results with two deep well data (San Donato 1 and Mt. Civitello 1 wells; https://www.videpi.com) drilled in the same formations and considering the same analysed depth interval, showing similar values between 20 Ωm and 30 Ωm, for the Marnoso-Arenacea Fm. (Fig. S3). We have also investigated the resistivity of the Schlier Fm. along the Canopo

1 well (https://www.videpi.com), although this latter is located far away from the study area, approximately 80 km NNE of Gubbio. Also in this case the resistivity values, around 7 Ωm, are comparable with our data (Fig. S3).

Information obtained from the velocity logs are more significant, including all 6 boreholes. We compared the Vp values recorded in the six shallow STAR boreholes (depth < 0.2 km, see Table 1) with data derived from sonic log analyses in much deeper wells (depth > 4 km) drilled in the same region for industrial purposes (Bigi et al., 2011; Scisciani et al., 2014; Montone and Mariucci, 2020; Trippetta et al., 2021). These studies report average Vp values between 4.0 km/s and 4.8 km/s for the Marnoso-Arenacea Fm., 4.4 km/s to 4.8 km/s for the Schlier Fm., 5.3 km/s to 5.8 km/s for the Scaglia Rossa Fm., and 5.5 km/s to 6.1 km/s for the Maiolica Fm. All these values are approximately 15% higher than our results but follow the same overall trend, with higher average Vp values recorded in the Maiolica and lower values in the Tertiary marly Formations. This increase in P-wave velocity with depth is primarily attributed to increased rock density and compaction, particularly in the Tertiary formations.

Due to a different degree of porosity linked to the different investigated depths and to the pore type, P-wave velocity can significantly change (e.g. Hairabian et al., 2014; Smeraglia et al., 2014; Trippetta et al., 2021). Moreover, P-wave velocity also depends on factors such as lithology changes, presence of fractures or faults and also on the different amount of tectonic deformation observed in different structural domains (Trippetta et al., 2021). Collecting and analysing the velocity data of upper crustal sedimentary rocks is very useful under different aspects. On one end, these values help building and calibrating more accurate 2D and 3D velocity models, that can be used for improving the earthquakes localization (e.g. Latorre et al., 2016; Montone and Mariucci, 2023) as well as to constrain depth conversion of seismic reflection profiles. On the other hand, since the velocity parameters of rocks are strictly related to their rigidity, velocity values also reflect their different mechanical behaviour and may ultimately influence earthquake generation and distribution. In our case, the more competent carbonate formations (i.e. Maiolica and Scaglia Rossa Fms.) are characterised by systematically higher velocities compared to less competent, clay-rich turbidite formations (i.e. Schlier and Marnoso-Arenacea Fms.).

In the ATF region, as well as in adjacent areas in the same seismotectonic framework of the Central Apennines, several recent studies of the relationships between seismicity distribution and upper crustal geological setting have been recently performed, by plotting accurately relocated seismic sequences on well-calibrated geological subsurface models, based on depth conversion of seismic reflection profiles (e.g. Latorre et al., 2016; Barchi et al., 2021; Collettini et al., 2022; Chiaraluce et al., 2017b). These studies coherently indicated that upper crustal seismicity (and the normal faulting earthquake mainshocks, in particular) are systematically hosted in the high velocity, Mesozoic or Early Tertiary successions, consisting of carbonates, dolostones and anhydrites, whilst only few, low magnitude events are recorded in the overlying, less competent Neogene turbidites, mainly consisting of marls and sandstones.

5.2 Stress Field

To constrain the orientation of the stress field in the area of the STAR project, we have analysed and interpreted the fractures detected in the six boreholes and compared them with the breakout orientations from the two deep wells and also with the other stress indicators, mainly focal mechanism data. In our boreholes, ABI and OBI images do not reveal any borehole breakouts. However, breakouts at very shallow depth could not be related or representative to the stress field because their occurrence would be linked to local effects such as topography, local faulting, folding, and other near-surface geological structures. As already mentioned, in the STAR study area (Fig. 2) two deep wells (SD and MC) were drilled in the past, reaching a depth of 4763 and 5600 m, respectively. The SD well is located very close to the ATF, intersecting it at a shallow depth; while the MC well, approximately 15 km east of the ATF fault, intersects additional tectonic structures. A thorough analysis of borehole breakout stress data conducted along the two deep wells, allowed to deduce the current stress field orientation (Mariucci et al., 2008). In the case of the SD well, the borehole breakout results reveal a minimum horizontal stress orientation of N055±22°; the MC well exhibits a slightly different stress orientation, with a value of N012±29° (Fig. 11).

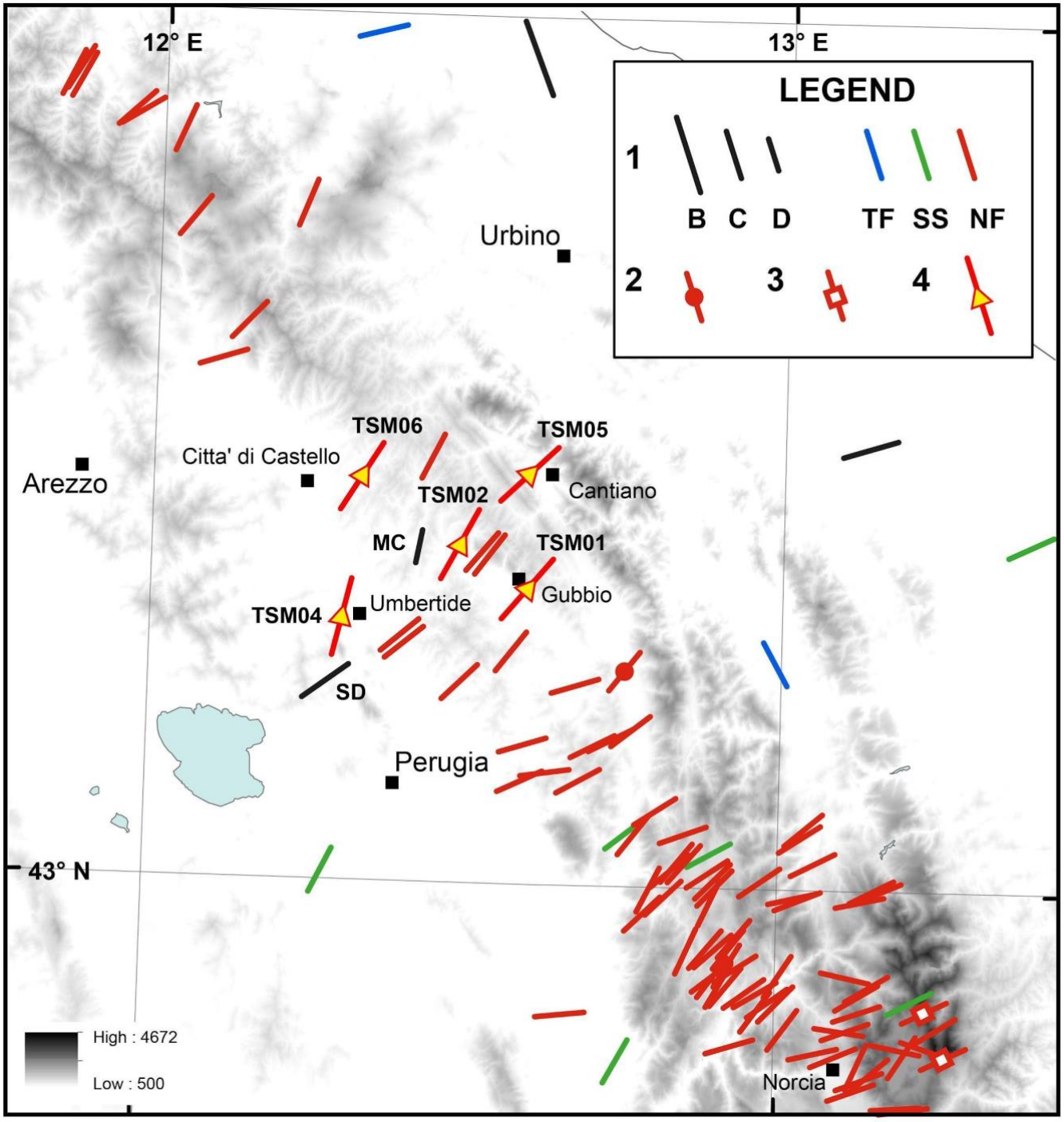
12° E
13° E
LEGEND
1
B C D TF SS NF
2
3
4
Urbino
TSM06
TSM05
Citta' di Castello
Arezzo
Cantiano
TSM02
MC
TSM01
Gubbio
TSM04
Umbertide
SD
Perugia
43° N
High : 4672
Low : 500
Norcia

Figure 11: Present-day stress field of Central Italy. The minimum horizontal stress orientations inferred both from the >45° dipping fractures detected along the STAR boreholes (bars with yellow triangles) and from the Italian Present-day Stress Indicators database IPSI 1.6 (Mariucci and Montone, 2024) are shown. 1- Borehole breakout (black bar) and focal mechanism (coloured bar) data; 2- formal inversion data; 3- fault data. All data are scaled by quality (from B to D) and coloured according to tectonic regime: black bar is unknown regime (breakout), blue is thrust faulting, green is strike-slip faulting, red is normal faulting. 4- data from TSM boreholes.

To interpret the structural data obtained along the STAR boreholes, we have considered i) the shallow depth of the boreholes, ii) their near-vertical inclination, that strongly underestimates occurrence of near-vertical features (Terzaghi, 1965; Massiot et al., 2015), and iii) the difficulty in distinguishing fractures from faults in this type of data.

Along the STAR boreholes, the main features with a dip angle > 45° (Fig. 10, column f) show a predominantly NW-SE orientation and could be interpreted as pre-existing fractures generated in the early phases of the deformation history before folding (Price, 1966).

Considering that the current stress field in the area is primarily due to an extensional regime, with the main compressional stress, sigma 1, vertical and horizontal sigma 3 NE-SW oriented, the tectonic structures associated with this latter stress field consequently develop normal faults and high-dip extensional fractures. These > 45° NW-SE structures, favourably oriented with respect to the current extensional stress field (Fig. 11), might have been reactivated as extensional fractures. In TSM04 and TSM06 boreholes, for structures with a dip greater than 45° (Fig. 10, column f), another orientation is also observed, approximately 90° from the previous one. We can assume that both fractures NW-SE and NE-SW oriented are contemporaneous and linked to the same extensional stress field, primarily guided by a vertical sigma 1. On the other hand, structures with low dip - still NW-SE oriented - could be attributed to previous compressive deformation phases linked to a stress field characterised by a horizontal sigma 1, oriented NE-SW. Taking into careful consideration the different depths investigated by the STAR boreholes (<0.2 km) with respect to the active stress data mainly inferred from breakout data in deep wells (0.5-6 km) and focal mechanisms of crustal earthquakes (usually 5-15 km), we can still compare their results (Fig. 11). In fact, most of the results from literature on the orientation of the stress field have shown that different crustal depths do not reorient or change the stress field (Heidbach et al., 2016; Mariucci and Montone, 2024). An almost constant orientation of the minimum horizontal stress characterises this sector of the Apennines, from the southern L'Aquila and Norcia zones to the areas north of Gubbio, showing only a slight rotation from ENE-NE directions to NE-NNE directions, respectively (Fig. 11). This is observed from numerous data derived from earthquake focal mechanisms as well as breakout data in deep wells, also present in the southernmost sector (Mariucci and Montone, 2016) and active fault data (Lavecchia et al., 2022), under a stress regime that can be defined as exclusively extensional.

In conclusion, our paper provides reliable values on physical properties of rocks, in particular P-wave velocity, which can be used to characterise crustal velocity models and allow detailed interpretation of seismic profiles, investigating the first two hundred metres of the crust. However, detailed geophysical measurements from shallow boreholes are relatively rare. A small, homogeneous rock sample analysed in the laboratory may not accurately represent the complexity of the in situ rock formation,

which can exhibit significant internal variability in composition and fracturing. Additionally, although our sites provide in situ measurements, they represent a relatively small dataset compared to the extensive data collected from deep well logs, which span hundreds of metres. This limitation could explain the discrepancies observed, such as the differences in Vp values. While our measured values are lower than the average data, they still fall within the acceptable range.

Beyond the specific case presented, our data significantly enhance our understanding of the upper crust. These in situ measurements bridge the gap between data from outcropping rocks and data from deeper wells. In particular, this scientific approach is able to provide useful geophysical information at the very shallow crustal depth (<0.2 km), typically not explored by either the scientific community or oil and gas industry. Our study demonstrates that even a limited dataset can provide valuable insights and represent possible case history for future projects. With an expanded dataset across a region of interest, it would be possible to illuminate a comprehensive section of the crust, extending from the surface to several kilometres deep, and potentially even deeper.

References

Amato, A. and Cocco, M. (eds): The Umbria-Marche, central Italy, Seismic Sequence of 1997–1998, Journal of Seismology, 4(4), 5–598, 2000.

Amato, A., Azzara, R., Chiarabba, C., Cimini, G. B., Cocco, M., Di Bona, M., Margheriti, L., Mazza, S., Mele, F., Selvaggi, G., Basili, A., Boschi, E., Courboulex, F., Deschamps, A., Gaffet, S., Bittarelli, G., Chiaraluce, L., Piccinini, D., and Ripepe, M.: The 1997 Umbria-Marche seismic sequence: a first look at the main shocks and aftershocks, Geophysical Research Letters, 25, 2861–2864, 1998.Anderlini, L., Serpelloni, E., and Belardinelli, M.: Creep and locking of a low-angle normal fault: Insights from the Altotiberina fault in the Northern Apennines (Italy), Geophysical Research Letters, 43, 4321–4329, https://doi.org/10.1002/2016GL068604, 2016.

Arthur, M. A. and Fischer, A. G.: Upper Cretaceous-Paleocene magnetic stratigraphy at Gubbio, Italy I. Lithostratigraphy and sedimentology, Geological Society of American Bulletin., 88, 367–371, 1977.

Barchi, M. R., De Feyter, A., Magnani, M.B., Minelli, G., Pialli, G. and Sotera, B. M.: The structural style of the Umbria-Marche fold and thrust belt, Memorie della Societá Geologica Italiana, 52, 557–578, 1998.

Barchi, M. R., Carboni, F., Michele, M., Ercoli, M., Giorgetti, C., Porreca, M., Azzaro, S., Chiaraluce, L.: The influence of subsurface geology on the distribution of earthquakes during the 2016-2017 Central Italy seismic sequence, Tectonophysics, 807, 22879, https://doi.org/10.1016/j.tecto.2021.228797, 2021.

Barchi, M. R. and Collettini, C.: Seismicity of central Italy in the context of the geological history of the Umbria-Marche Apennines, Special Paper of the Geological Society of America, 542, 175 – 190, 2019.

Barchi, M. R. and Mirabella, F.: The 1997-98 Umbria-Marche earthquake sequence: "Geological" vs. "seismological" faults, Tectonophysics, 476(1-2), 170-179, 10.1016/j.tecto.2008.09.013 (2009).

Barchi, M. R.: The Neogene-Quaternary evolution of the Northern Apennines: crustal structure, style of deformation and seismicity, Journal of the Virtual Explorer, 36, 2010.

Bigi, S., Casero, P., and Ciotoli, G.: Seismic interpretation of the Laga basin; constraints on the structural setting and kinematics of the Central Apennines, Journal of Geological Society of London, 168, 179–190, https://doi.org/10.1144/0016-76492010-084, 2011.

Bohnhoff, M., Dresen, G., Ceken, U., Kadirioglu, F. T., Kartal, R. F., Kilic, T., Nurlu, M., Yanik, K., Acarel, D., Bulut, F., Kloth, A., Johnson, W., Malin, P. and, Mencin, D.: GONAF – the borehole Geophysical Observatory at the North Anatolian Fault in the eastern Sea of Marmara, Scientific Drilling: reports on deep earth sampling and monitoring, 22, 19-28, https://doi.org/10.5194/sd-22-19-2017, 2017.

Boncio, P. and Lavecchia, G.: A geological model for the Colfiorito earthquakes (September–October 1997, central Italy), Journal of Seismology, 4, 345–356, 2000.

Boncio, P., Pizzi, A., Brozzetti, F., Pomposo, G. Lavecchia, G., Di Naccio, D., Ferrarini, F.: Coseismic ground deformation of the 6 April 2009 L'Aquila earthquake (central Italy, Mw6.3), Geophysical Research Letters, 37, L06308, 2010.

Caricchi, C., Aldega, L., Barchi, M. R., Corrado, S., Grigo, D., Mirabella, F., Zattin, M.: Exhumation patterns along shallow low-angle normal faults: an example from the Altotiberina active fault system (Northern Apennines, Italy), Terra Nova, 27, 312–321, https://doi.org/doi:10.1111/ter.12163, 2015.

Cello, G., Mazzoli, S., Tondi, E., and Turco, E.: Active tectonics in the central Apennines and possible implications for seismic hazard analysis in peninsular Italy, Tectonophysics, 272, 43–68, http://dx.doi.org/10.1016/S0040-1951(96)00275-2, 1997.

Chiarabba, C., De Gori, P., Cattaneo, M., Spallarossa, D., and Segou, M.: Faults geometry and the role of fluids in the 2016-2017 Central Italy seismic sequence, Geophys. Res. Lett., 45, 6963–6971, https://doi.org/10.1029/2018GL077485, 2018.

Chiarabba, C., Jovane, L., and Di Stefano, R.: A new view of Italian seismicity using 20 years of instrumental recordings, Tectonophysics, 305, 251–268, 2005.

Chiaraluce, L., Di Stefano, R., Tinti, E., Scognamiglio, L., Michele, M., Casarotti, E., Cattaneo, M., De Gori, P., Chiarabba, C., Monachesi, G., Lombardi, A., Valoroso, L., Latorre, D., Marzorati, S.: The 2016 Central Italy seismic sequence: a first look at the mainshocks, aftershocks, and source models, Seismological Research Letters, 88(3), 757–771, https://doi.org/10.1785/0220160221, 2017b.

Chiaraluce, L., Amato, A., Carannante, S., Castelli, V., Cattaneo, M., Cocco, M., Collettini, C., D'Alema, E., Di Stefano, R., Latorre, D., Marzorati, S., Mirabella, F., Monachesi, G., Piccinini, D., Nardi, A., Piersanti, A., Stramondo, S., and Valoroso, L.: The Alto Tiberina Near Fault Observatory (northern Apennines, Italy), Annals of Geophysics, 57, S0327, https://doi.org/10.4401/ag-6426, 2014a.

Chiaraluce, L., Festa, G., Bernard, P., Caracausi, A., Carliccio, I., Clinton, j., Di Stefano, R., Elia, L., Evangelidis, C., Ergintav, S., Jianu, O., Kaviris, G., Marmureanu, A., Sebela., S., and Sokos, E.: The Near Fault Observatory community in Europe: a new resource for faulting and hazard studies, Annals of Geophysics, 65(3), https://doi.org/10.4401/ag-8778, 2022.

Chiaraluce, L., Festa, G., Bernard, P., Caracausi, A., Carluccio, I., Clinton, J.F., Di Stefano, R., Elia, L., Evangelidis, C.P., Ergintav, S., Jianu, O., Kaviris, G., Marmureanu, A., Šebela, S., and Sokos, E.: The role of rheology, crustal structures and lithology in the seismicity distribution of the northern Apennines, Tectonophysics, 694, 280–291. https://doi.org/10.1016/j.tecto.2016.11.011, 2017a.

Chiaraluce, L., Collettini, C., Cattaneo, M., and Monachesi, G.: The shallow boreholes at the Altotiberina near fault Observatory (TABOO; northern Apennines of Italy), Scientific Drilling, 17, 31–35, https://doi.org/10.5194/sd-17-31-2014, 2014b.

Chiaraluce, L., Ellsworth, W. L., Chiarabba, C., and Cocco, M.: Imaging the complexity of an active normal fault system: The 1997 Colfiorito (Central Italy) case study, Journal of Geophysical Research, 108(B6), https://doi.org/10.1029/2002JB002166, 2003.

Chiaraluce, L. Bennett, R., Mencin, D., Johnson, W., Barchi, M.R., Bohnhoff, M., Baccheschi, P., Caracausi, A., Calamita, C., Cavaliere, A., Gualandi, A., Mandler, E., Mariucci, M.T., Martelli, L., Marzorati, S., Montone, P., Pantaleo, D., Pucci, S., Serpelloni, E., Supino, M, Stramondo, S., Hanagan, C., Van Boskirk, L., Gottlieb, M., Mattioli, G., Urbani, M., Mirabella, F., Akimbekova, A., Pierdominici, S., Wiersberg, T., Chris Marone, C., Palmieri, L., and Schenato, L.: A Strainmeter Array as Fulcrum of Novel Observatory Sites Along the Alto Tiberina Near Fault Observatory, Scientific Drilling, 33, 173-190, https://doi.org/10.5194/sd-33-173-2024, 2024.

Ciaccio, M.G., Barchi, M.R., Chiarabba, C., Mirabella, F., and Stucchi, E.: Seismological, geological and geophysical constraints for the Gualdo Tadino fault, Umbria–Marche Apennines (central Italy), Tectonophysics, 406(3-4), 233-247, https://doi.org/10.1016/j.tecto.2005.05.027, 2005.

Cinti, F. R., Cucci, L., Marra, F., and Montone, P.: The 1997 Umbria-Marche (Italy) earthquake sequence: Relationship between ground deformation and seismogenic structure, Geophysical Research Letters, 26, 895–898, 1999.

Collettini, C., Barchi, M. R., De Paola, N., Trippetta, F., and Tinti, E.: Rock and fault rheology explain differences between on fault and distributed seismicity, Nature communication, 13, 5627, https://doi.org/10.1038/s41467-022-33373-y, 2022.

Cresta, S., Monechi, S., and Parisi, G.: Stratigrafia del Mesozoico al Cenozoico nell'area Umbro-Marchigiana, Memorie Descrittive della Carta Geologica d´Italia, 34, 185, 1989.

Davatzes, N.C. and Hickman, S.H.: Stress, fracture, and fluid-flow analysis using acoustic and electrical image logs in hot fractured granites of the Coso geothermal field, California, U.S.A., in M. Poppelreiter, C. Garcia-Carballido, and M. Kraaijveld, eds., Dipmeter and borehole image log technology. AAPG Memoir 92, p. 259 – 293, 2010.

De Paola, N., Faulkner, D.R., and Collettini, C.: Brittle versus ductile deformation as the main control on the transport properties of low-porosity anhydrite rocks, Journal of Geophysical Research, 114, B06211, http://dx.doi.org/10.1029/2008JB005967, 2009.

Deschamps, A., Iannaccone, G., and Scarpa, R.: The Umbrian earthquake (Italy) of 19 September 1979, Annales Geophysicae, 2(1), 29-36, 1984.

Diaferia, I., Barchi, M., Loddo, M., Schiavone, D., and Siniscalchi, A. Detailed imaging of tectonic structures by multiscale Earth resistivity tomographies: The Colfiorito normal faults (central Italy). Geophys. Res. Lett., 33, L09305, doi:10.1029/2006GL025828, 2006

Ellis D.V. and Singer J.M.: Well Logging for Earth Scientists. 2nd edition Springer, pp 699, 2007.

EMERGEO Working Group: Evidence for surface rupture associated with the Mw 6. 3 L'Aquila earthquake sequence of April 2009 (central Italy), Terra Nova, 22, 43–51, 2010.

Fischer, T., Hrubcová, P., Dahm, T., Woith, H., Vylita, T., Ohrnberger, M., Vlček, J., Horálek, J., Dedeček, P., Zimmer, M., Lipus, M., Pierdominici, S., Kallmeyer, J., Krüger, F., Hannemann, K., Korn, M., Kämpf, H., Reinsch, T., Klicpera, J., Volmer, D., Daskalopoulou, K. (2022). ICDP Eger Rift observatory: Magmatic Fluids Driving the Earthquake Swarms and Deep Biosphere - Scientific and technological achievements, Scientific Drilling, 31, 31-49, https://doi.org/10.5194/sd-31-31-2022.

Haessler, H., Gaulon, R., Rivera, L., Console, R., Frogneux, M., Gasparini, G., Martel, L., Patau, G., Siciliano, M., and Cisternas, A.: The Perugia (Italy) earthquake of 29 April 1984: a microearthquake survey, Bulletin of the Seismological Society of America, 78, 1948–1964, 1988.

Hairabian, A., Fournier, F., Borgomano, J., and Nardon, S.: Depositional facies, pore types and elastic properties of deep-water gravity flow carbonates Journal of Petroleum Geology, 37, 231–249, 2014.

Heidbach, O., Rajabi, M., Reiter, K., Ziegler, M., and WSM Team: World Stress Map Database Release 2016. V. 1.1, GFZ Data Services, https://doi.org/10.5880/WSM.2016.001, 2016.

Italian CMT dataset (http://www.bo.ingv.it/RCMT/Italydataset.html)

Langbein, J., Murray, J.R., and Snyder, H.A.: Coseismic and initial postseismic deformation from the 2004 Parkfield, California, earthquake, observed by Global Positioning System, electronic distance meter, creepmeters, and borehole strainmeters, Bulletin of the Seismological Society of America, 96(4B), S304-S320, 2006.

Latorre, D., Mirabella, F., Chiaraluce, L., Trippetta, F., and Lomay, A.: Assessment of earthquake locations in 3-D deterministic velocity models: A case study from the Altotiberina Near Fault Observatory (Italy), Journal of Geophysical Research: Solid Earth, 121(11), 8113-8135, https://doi.org/10.1002/2016JB013170, 2016.

Lavecchia, G., Adinolfi, G. M., de Nardis, R., Ferrarini, F., Cirillo, D., Brozzetti, F., De Matteis, R., Festa, G., and Zollo, A.: Multidisciplinary inferences on a newly recognized active east-dipping extensional system in Central Italy, Terra Nova, 29, 77–89, 2017.

Lavecchia, G., Bello, S., Andrenacci, C., Cirillo, D., Ferrarini, F., Vicentini, N., de Nardis, R., Roberts, G., Brozzetti, F.: Quaternary fault strain INdicators database - QUIN 1.0-first release from the Apennines of central Italy, Scientific Data, 9(1), doi 10.1038/s41597-022-01311-8, 2022.

Mariucci M.T. and Montone P.: Contemporary stress field in the area of the 2016 Amatrice seismic sequence (central Italy), Annals of Geophysics, 59, fast track 5, doi:10.4401/ag-7235, 2016.

Mariucci M.T., Montone P., and Pierdominici S.: Active stress field in central Italy: a revision of deep well data in Umbria region, Annals of Geophysics, 51, 2/3, 433-442, 2008.

Mariucci, M.T. and Montone, P.: IPSI 1.6, Database of Italian Present-day Stress Indicators, Istituto Nazionale di Geofisica e Vulcanologia (INGV), http://doi.org/10.13127/IPSI.1.6, 2024.

Marzorati, S., Massa, M., Cattaneo, M., Monachesi, G., and Frapiccini, M.: Very detailed seismic pattern and migration inferred from the April 2010 Pietralunga (northern Italian Apennines) micro-earthquake sequence, Tectonophysics, 610, 91–109, https://doi.org/10.1016/j.tecto.2013.10.014, 2014.

Massiot, C., McNamara, D., and Lewis, B.: Processing and analysis of high temperature geothermal acoustic borehole image logs in the Taupo Volcanic Zone, New Zealand, Geothermics, 53, 190–201, https://doi.org/10.1016/j.geothermics.2014.05.010, 2015.Mcginnis, R. N., Ferrill, D. A., Morris, A. P., Smart, K. J. and Lehrmann, D.: Mechanical stratigraphic controls on natural fracture spacing and penetration, Journal of Structural Geology, 95, 160–170, https://doi.org/10.1016/j.jsg.2017.01.001, 2017.

Medici, G, Ling F., and Shang, J.: Review of discrete fracture network characterization for geothermal energy extraction, Frontiers Earth Science, 11, 1328397, https://doi.org/10.3389/feart.2023.1328397, 2023.

Michele, M., Chiaraluce, L., Di Stefano, R., and Waldhauser, F.: Fine-Scale Structure of the 2016–2017 Central Italy Seismic Sequence From Data Recorded at the Italian National Network, Journal of Geophysical Research, 125, e2019JB01844, https://doi.org/10.1029/2019JB018440, 2020.

Mildon, Z. K., Roberts, G. P., Faure Walker, J. P., Wedmore, L. N. J., and McCaffrey, K. J. W.: Active normal faulting during the 1997 seismic sequence in Colfiorito, Umbria: Did slip propagate to the surface?, Journal of Structural Geology, 91, 102–113, 2016.

Mirabella, F., Brozzetti, F., Lupattelli, A., and Barchi, M.R.: Tectonic evolution of a low-angle extensional fault system from restored cross-sections in the Northern Apennines (Italy), Tectonics, 30, TC6002, doi:10.1029/2011TC002890, 2011.

Mirabella, F., Ciaccio, M.G., Barchi, M.R., and Merlini, S.: The Gubbio normal fault (Central Italy): geometry, displacement distribution and tectonic evolution, Journal of Structural Geology, 26, 2233-2249, doi:10.1016/j.jsg.2004.06.009, 2004.

Montone, P. and Mariucci, M. T.: The new release of the Italian contemporary stress map, Geophysical Journal International, 205, 1525–1531, https://doi.org/10.1093/gji/ggw100, 2016.

Montone, P. and Mariucci, M.T.: Constraints on the Structure of the Shallow Crust in Central Italy from Geophysical Log Data, Scientific Reports, 10, 3834, https://doi.org/10.1038/s41598-020-60855-0, 2020.

Montone, P. and Mariucci M.T.: Lateral Variations of P-Wave Velocity from Deep Borehole Data in the Southern Apennines, Italy, Pure and Applied Geophysics, 180, 1925–1944, https://doi.org/10.1007/s00024-023-03248-4, 2023.

Pierdominici, S. and Kück, J.: Borehole Geophysics. In: Encyclopedia of Geology (Second Edition), Elsevier, 746-760, https://doi.org/10.1016/B978-0-08-102908-4.00126-0, 2021.

Pierdominici, S., Millett, J. M., Kück, J. K. M., Thomas, D., Jerram, D. A., Planke, S., Haskins, E., Lautze, N., and Galland, O.: Stress field interactions between overlapping shield volcanoes: Borehole breakout evidence from the island of Hawaii, USA, Journal of Geophysical Research, 125, e2020JB019768, https://doi.org/10.1029/2020JB019768, 2020.

Pizzi, A., Di Domenica, A., Gallovic, F., Luzi, L., and Puglia, R.: Fault segmentation as constraint to the occurrence of the main shocks of the 2016 Central Italy seismic sequence, Tectonics, 36, 2370–2387, https://doi.org/10.1002/2017TC004652, 2017.

Pondrelli, S. and Salimbeni, S.: Italian CMT Dataset (Data set). Istituto Nazionale di Geofisica e Vulcanologia (INGV), https://doi.org/10.13127/rcmt/italy, 2006.

Pondrelli, S., Salimbeni, S., Ekström, G., Morelli, A., Gasperini, P., and Vannucci, G.: The Italian CMT dataset from 1977 to the present, Physics of the Earth and Planetary Interiors, 159(3-4), 286-303, doi:10.1016/j.pepi.2006.07.008, 2006.

Porreca, M., Minelli, G., Ercoli, M., Brobia, A., Mancinelli, P., Cruciani, F., Giorgetti, C., Carboni, F., Mirabella, F., Cavinato, G., Cannata, A., Pauselli, C., and Barchi, M. R.: Seismic reflection profiles and subsurface geology of the area interested by the 2016–2017 earthquake sequence (Central Italy), Tectonics, 37, 1116–1137, https://doi.org/10.1002/2017TC004915, 2018.

Price, N.J. Fault and Joint Development in Brittle and Semi-Brittle Rocks. Pergamon Press, Oxford, 1966 Quick Regional Moment Tensors, http://autorcmt.bo.ingv.it/quicks.html

Rider, M.H. and Kennedy, M.: The Geological Interpretation of Well Logs, 432 pp, Rider-French, Scotland, 2011.

Schön, J.H.: Physical Properties of Rocks - Fundamentals and Principles of Petrophysics. 2nd Edition -Elsevier, 2015.

Scisciani, V., Agostini, S., Calamita, F., Pace, P., Cilli, A., Giori, I., and Paltrinieri, W.: Positive inversion tectonics in foreland fold-and thrust belts: a reappraisal of the Umbria–Marche northern Apennines (Central Italy) by integrating geological and geophysical data, Tectonophysics, 637, 218–237, https://doi.org/10.1016/j. tecto.2014.10.010, 2014.

Serra, O.: Fundamentals of well-log interpretation. Part 1: The acquisition of logging data. Developments in petroleum science 15A, Amsterdam, Elsevier, pp 435, 1984.

Smeraglia, L., Trippetta, F., Carminati, E., and Mollo, S.: Tectonic control on the petrophysical properties of foredeep sandstone in the Central Apennines, Italy, Journal of Geophysical Research, 119, 9077–9094, 2014.

Terzaghi, R. D.: Sources of error in joint surveys, Geotechnique, 15(3), 287–304, https://doi.org/10.1680/geot.1965.15.3.287, 1965.

Tinti, E., Scognamiglio, L., Michelini, A., and Cocco, M.: Slip heterogeneity and directivity of the ML 6.0 2016 Amatrice earthquake estimated with rapid finite-fault inversion, Geophysical Research Letters, 43(10), 10,745–10,752, https://doi.org/10.1002/2016GL071263, 2016.

Trippetta F., Barchi, M. R., Tinti, E., Volpe, G., Rosset, G., and De Paola, N.: Lithological and stress anisotropy control large-scale seismic velocity variations in tight carbonates, Scientific Reports, 11, 9472, https://doi.org/10.1038/s41598-021-89019-4, 2021.

Trippetta, F., Collettini, C., Vinciguerra, S., and Meredith, P.G.: Laboratory measurements of the physical properties of Triassic evaporites from central Italy and correlation with geophysical data, Tectonophysics, 492, 121–132, http://dx.doi.org/10.1016/j.tecto.2010.06.001, 2010.

Valoroso, L., Chiaraluce, L., Di Stefano, R., and Monachesi, G.: Mixed-mode slip behaviour of the Altotiberina low-angle normal fault system (Northern Apennines, Italy) through high-resolution earthquake locations and repeating events, Journal of Geophysical Research: Solid Earth, 122, https://doi.org/10.1002/2017JB014607, 2017.

Valoroso, L., Chiaraluce, L., Piccinini, D., Di Stefano, R., and Waldhauser, F.: Radiography of a normal fault system by 64,000 high-precision earthquake locations: The 2009 L'Aquila (central Italy) case study, Journal of Geophysical Research: Solid Earth, 118, 1156-1176, https://doi.org/10.1002/jgrb.50130, 2013.

Villani, F., Civico, R., Pucci, S., Pizzimenti, L., Nappi, R., De Martini, P. M., and the Open EMERGEO Working Group: A database of the coseismic effects following the 30 October 2016 Norcia earthquake in Central Italy, Scientific Data, 5, 180049, https://doi.org/10.1038/sdata.2018.49, 2018.

Vuan, A., Brondi, P., Sugan, M., Chiaraluce, L., Di Stefano, R., and Michele, M.: Intermittent slip along the Alto Tiberina low angle normal fault in central Italy, Geophysical Research Letters, 47, e2020GL08903, https://doi.org/10.1029/2020GL089039, 2020.

Data Availability

The downhole logging dataset and additional information about the boreholes are available at the ICDP repository database (https://www.icdp-online.org/projects/by-continent/europe/star-italy/public-data/).

Author Contributions

Author Contributions: PM, SP, MRB conceptualization, methodology; PM, SP, MTM, AA formal analysis; PM, SP, MTM, LC, MU, FM, WJ field investigation; LC, AA, MU, FM data curation; PM, SP, MRB, MTM writing—original draft preparation; SP, MU, MTM visualisation; PM, SP, MRB, MTM writing—review and editing. All co-authors contributed to reviewing and revising the paper. All authors have read and agreed to the published version of the manuscript.

Competing Interests

The authors declare that they have no conflict of interests.

Acknowledgments

GEOTEC (http://geo-tec.it/en/) and GEOLOGIN Srl (https://www.geolog-in.com/) are thanked for providing drillings and geophysical borehole log data. We are grateful to Earthscope for providing strainmeters. STAR drilling project is co-funded by the International Continental Scientific Drilling Program (ICDP), by the United States National Science Foundation (NSF) and by the Italian Istituto Nazionale di Geofisica e Vulcanologia (INGV).

Supplementary Material

See Supplementary file